Title

Visualizing a Dynamic Allosteric Network in Human Herpesvirus Proteases with an Inhibitory Antibody

Permalink

https://escholarship.org/uc/item/9vr1n8jd

Author

Zimanyi, Marcell Antal

Publication Date

2024

Peer reviewed|Thesis/dissertation

Visualizing a Dynamic Allosteric Network in Human Herpesvirus Proteases with an Inhibitory Antibody
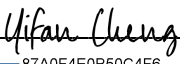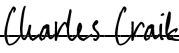
by
Marcell Antal Zimanyi

DISSERTATION
Submitted in partial satisfaction of the requirements for degree of
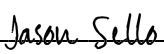DOCTOR OF PHILOSOPHY

in

Chemistry and Chemical Biology

in the

GRADUATE DIVISION
of the
UNIVERSITY OF CALIFORNIA, SAN FRANCISCO

Approved:

Acknowledgments

This work would not have been possible without the support of many. I will remember my time at UCSF as a period of learning, growth, and creativity, and I have many mentors, peers, family, and friends to thank.

I would like to thank my advisor, Yifan Cheng, for his support and mentorship. You gave me the tools and freedom to explore questions in a field that was new to me, and when things didn't work out, your encouragement and pragmatism kept me on track. You show the world that electron microscopy is a technique full of wonder, and I greatly appreciate the opportunity to wield it. Yifan's leadership style cultivates a culture of progress because he assembles creative and talented people and removes obstacles from their path. This leads me to thank my peers in the Cheng lab, past and present, for your support. The deep camaraderie I have felt working together inspired me to be a better scientist and filled my soul with friendship, and you all have taught me so much. Daniel Asarnow, you shaped my understanding of how to investigate using electron microscopy, and how to have fun at every turn. Caleigh Azumaya, your kindness and positivity made me feel so welcome when I first joined the lab, and I appreciate that you taught me how to use the microscopes! Will Arnold, I will always remember the silliness and levity we shared in the lab, but I will also note that you are a rigorous and talented scientist who taught me a great deal. To Adamo Mancino, Maxine Bi, Estelle Ronane, and Kevin Chung; I am so glad we could share the adventure of graduate school and support each other through the highs and lows. To Wooyoung Choi, Jinsung Kim, MJ (Mingliang Jin), Hao Wu, John Wang and Jiahua He, you shared with me great scientific engagement and support along with a friendship that made me excited to come to work every day.

I would also like to thank Charles Craik for his mentorship and support. Charly, you have been a tireless advocate in my career ever since we met, and your belief in my capabilities helped me unlock them in myself. Our adventures to California's mountains, vineyards, and

iii

restaurant scene have cemented a friendship I will treasure as much as your mentorship. I would also like to thank members of the Craik lab for their support and friendship. You all showed me the terrifying beauty of the graduate school experience and gave me the tools I needed to try it myself. To Kaitlin Hulce, the symbolic second author of this thesis, I would like to express appreciation for your genuine kindness and your relentless investigative determination. To Markus Bohn, you inspired me to become a structural biologist. You just made it look so cool! I appreciate your ambition to reveal the scientific connections between seemingly disparate observations, and I appreciate your way of pulling me towards the middle. Namely, you reminded me to be skeptical when things worked out, and optimistic and creative when they did not. I would also like to give special thanks to Peter Rohweder who has been a prominent guiding force in my life since we met. I respect your scientific ambition as deeply as I treasure our friendship, and it has been an honor to spend the last eight years together.

I would also like to thank Jason Sello, the third member of my thesis committee. Jason, your warmth and attentiveness made me feel heard when I was tackling the challenging moments of my graduate tenure. Then, after hearing me out, you guided me toward taking a hard look at my research path on multiple occasions by cutting to the core of the problem. This clarity and encouragement have been formative. To my CCB cohort, you are such a cool group to have shared this experience with. You are a unique band of talented, hardworking, and fun people, and you have been an endless source of laughs and inspiration.

My family in both California and Hungary has been a perpetual source of both professional and scientific inspiration and support. To my mother Ildiko Antal, who is as caring as she is tenacious, thank you for instilling in me a humble ambition that keeps me going. Furthermore, you empower me with the drive to just get it done. To my father, Gergely Zimanyi, whose bottomless drive to create radiates in all directions, thank you for being a seminal

example of altruistic achievement. You showed me how to expect the best from myself both scientifically and socially, and you continue to be an example of how to make time for fun.

To my partner Lynnea Ormiston, thank you for taking the plunge with me. I am so fortunate for the love and friendship we share, and I appreciate your care and support through this journey. You are funny, clever, and imaginative, and your moral compass is the truest I know. I love you so much.

Contributions

This thesis contains soon-to-be-published results. These do not represent the final results and may be edited compared to published works.

Some data in Chapter 2 have been previously published in:

Hulce, K. (2021). Exploiting conformational dynamics to inhibit human herpesvirus proteases. *UCSF*. ProQuest ID: Hulce_ucsf_0034D_12165. Merritt ID: ark:/13030/m5pp571q. Retrieved from https://escholarship.org/uc/item/94j6r75v

Kaitlin Hulce, Marcell Zimanyi, Markus Bohn, Gregory Lee, and Charles designed the studies and wrote the manuscript. K.H, M.Z. and M.B. conducted biochemical experiments and generated reagents. M.Z. conducted and interpreted X-ray footprinting and cryo-electron microscopy experiments. K.H. and G.L. performed and analyzed nuclear magnetic resonance experiments.

Visualizing a Dynamic Allosteric Network in Human Herpesvirus Proteases with an Inhibitory Antibody

Marcell Zimanyi

Abstract

Exploiting conformational dynamics is a powerful method for inhibiting enzymes and can produce new allosteric inhibitors for managing disease. In this work, we outline the discovery and characterization of an antibody fragment called Fab5 which inhibits the human Cytomegalovirus protease (HCMV Pr). Using ensemble biophysical techniques, we describe the dynamic relationship between Fab5 and HCMV Pr, from which we propose a mechanism of inhibition along with potential insights into the broader conformational network that controls all human Herpesvirus Protease (HHV Pr) activation. Mutagenesis and biochemical characterization allow us to validate our hypotheses *in vitro.* We provide novel tools and strategies for HHV Pr inhibition that we believe can be leveraged in future therapeutic development. In Chapter 1.1, we use cryogenic electron microscopy (cryo-EM) to reveal the Fab5 binding site on HCMV Pr which we call the Latch Loop. We propose that Fab5 inhibits HCMV Pr by preventing dimerization through an allosteric mechanism that is both mechanistic and dynamic, ultimately preventing the protease from activating. Mutagenic studies demonstrate the previously unrecognized importance of the Latch Loop in the conformational network that links dimerization to HHV Pr activation. In Chapter 1.2, we use X-ray radiolytic Footprinting to survey solvent accessibility changes on HCMV Pr after Fab5 binding. These studies reveal a residue network near the HCMV Pr active site that influences dimerization and, thus, activity despite being buried in the center of the protease.

Table of Contents

List of Figures

List of Tables

Chapter 1

Antibody Inhibition of Human Cytomegalovirus Protease Via a Conserved Motif

Abstract

The human herpesviruses (HHVs) are a neglected family of pathogens that cause serious illness and currently infect over 90% of the global population. The viral lifecycle depends on the activity of the human herpesvirus maturational protease (HHV Pr), and loss of proteolysis arrests the lifecycle and disables viral egress. Using human cytomegalovirus protease (HCMV Pr), we panned for antibody fragments (Fabs) that bind to HCMV Pr and disrupt proteolysis. We identified a Fab termed Fab5 that inhibits proteolytic activity and disrupts dimerization by engaging a cryptic surface antipodal to the HCMV Pr active site. Our cryo-electron microscopy structures of the HCMV Pr/Fab5 complex reveal that Fab5 prevents proper packing of the HCMV Pr C-terminus, thus disrupting helices that facilitate active site coordination and homodimerization. We identified a three-residue motif called the C-terminal latch that is conserved across most HHV Prs, and we determined that mutating any of these residues to alanine ablates HCMV Pr activity and disrupts dimerization. Structural and functional characterization of Fab5 reveals that C-terminal latch disruption is a viable strategy for allosteric HHV Pr inhibitor development and could have broader implications for potential antibody-based HHV neutralization via cellular delivery.

Introduction

Human herpesviruses (HHVs) cause lifelong infections and are seroprevalent in over 90% of the global population.[1] Several serious diseases are associated with HHV infection, including encephalitis and certain cancers, and links between HHV infection and neurodegeneration have been suggested. In particular, human Cytomegalovirus (HCMV) represents a significant unmet clinical need. Although infected immunocompetent adults may never experience symptoms, immunocompromised individuals such as organ transplant recipients, HIV patients, and patients with autoimmune disease undergoing immunosuppressant treatments are at risk of life-threatening acute infections, and infants with congenital CMV infection can develop lifelong congenital disabilities or end-organ failure.[2–5] Current antivirals available to manage HHV infection suffer from toxicity and emergent resistance, and the only available HHV vaccine is against the Varicella-Zoster virus to prevent chickenpox and shingles.[1,6] Developing new HHV antiviral therapies is thus critically necessary to treat this neglected viral family.

All HHVs express a structurally conserved serine protease (HHV Pr), which facilitates viral capsid maturation.[7,8] Due to their essential role in viral replication, HHV Prs are a promising target for viral neutralization. HHV Pr is expressed with the assembly protein (AP) as a monomeric fusion (Pr-AP) in the host cytosol and translocates into the nucleus along with the major capsid protein (MCP), where it becomes enclosed in procapsids (**Fig. 1.1a**).[1] Not all APs are fused with a Pr due to multiple open reading frames in the UL80 gene (**Fig. 1.2**), and the C-terminal region of the Pr domain and most of the AP are thought to be disordered in monomeric states.[9]

Proteolysis is regulated by concentration-dependent HHV Pr homodimerization via weak, micromolar affinity self-association. This ensures protease activity occurs only within the capsid where the local HHV Pr concentration is high enough to promote dimerization.[10–12] Crystal structures of wild-type HCMV Pr are dimeric (**Fig. 1.1b**) and reveal a Ser-His-His catalytic triad, an oxyanion hole loop, and a dimerization interface comprised of major helices α5 and α1. Studies of the Pr domain *in vitro* showed that homodimerization initiates a disorder-to-order structural transition that orders the C-terminal region, which includes major helices α5 and α6, which packs beneath the protease active site (**Fig. 1.1c**).[12,13] These structural changes stabilize the oxyanion hole loop, leading to a catalytically competent active site on each monomer.[9] Once dimerized, HHV Prs free themselves from the AP by cleaving a release site (R-site) at the C-terminus of the Pr domain. This process likely happens in trans due to the distance between the release and active sites, coupled with the structural constraints required for activity.[1] This limits the premature release of HHV Pr before Pr-AP is incorporated into a procapsid. Once released, Pr cleaves the maturational site (M-site) on the AP leading to clearance of the scaffolding and ultimately capsid maturation.

Due to the active site's dynamic and shallow nature, efforts to develop active site inhibitors of HHV Prs have not yielded clinical candidates. An alternative approach to HHV Pr inhibition is interference with the conformational transition that ties dimerization to catalytic competency. We previously identified broad-spectrum small molecules that inhibit multiple HHV Prs by exploiting their conformational equilibrium. Compound DD2 occupies a pocket directly behind helix α5, which prevents the dimer interface from forming.[14–17] Compound **43** is an irreversible inhibitor that targets a conserved cysteine

near the HHV Pr active site, and it stabilizes the HCMV Pr dimer in a nonproductive state.[18] While both of these compounds leverage promising mechanisms of inhibition, they face unique challenges for development into high-potency drug leads, including solubility, specificity, and cell permeability. Recombinant antibodies (Abs) are particularly well suited to stabilizing conformational states of proteins, and they exhibit exquisite selectivity and potency for their targets.[19] Abs have been used to uncover novel mechanisms for protease inactivation, including non-canonical substrate pocket binding, disruption of dimerization or oligomerization, and uncovering new allosteric inhibitory sites.[20–23] This presents an alternative method to disrupt HHV Pr activity by identifying Abs that stabilize the protease in inactivated conformations, with particular focus on disruption of HHV Pr dimerization. While the therapeutic application of Abs has long been considered limited to extracellular targets, new advances in adeno-associated virus (AAV) gene transfer technology make intracellular delivery of Abs possible.[24,25] This opens the door to developing Ab-based biologics targeting intracellular HHV Prs to neutralize viral replication. An Ab could also reveal new druggable binding pockets on HHV Prs that can be exploited for therapeutic development, and there is potential that a single antibody could be broadly neutralizing across multiple HHV homologs.

In this work, we screened a phage-displayed Fab library and isolated a lead candidate termed Fab5, which can completely inhibit HCMV Pr activity *in vitro*.[26] Size-exclusion chromatography and multi-angle light scattering (SEC/MALS) revealed that Fab5 isolates HCMV Pr monomers. Solving a cryo-EM structure of the Fab5/HCMV Pr complex allowed us to model the Fab5 epitope, and a comparison to published dimeric HCMV Pr crystal structures revealed that Fab5 binds a cryptic site only available on the

HCMV Pr monomer. Fab5 disrupts a motif we termed the C-terminal latch, and mutating the three key residues that comprise the latch to alanine disrupts both HCMV Pr dimerization and activity. This latch motif is structurally conserved in all nine HHV Prs, and the key sidechains on the HCMV Pr latch are conserved across two-thirds of the HHV family. Mutating the latch residues in Kaposi's Sarcoma-associated virus (KSHV) and Eppstein-Barr virus also disrupts protease activity, which demonstrates that the C-terminal latch is a molecular switch that can be exploited to neutralize protease activity.

Results

Identification of an inhibitory antibody fragment against HCMV Pr

Using a phage-displayed naïve human B-cell derived Fab library, we identified five unique Fabs that recognize HCMV Pr (**Fig. 1.3**). We immobilized HCMV Pr on magnetic beads at low protein concentration to bias binders toward the monomeric species.[26,27] We used a synthesized peptide substrate with a donor/quencher pair to monitor *in vitro* HCMV Pr activity in the presence of each purified Fab. Two showed no effect on HCMV Pr activity (Fab1 and Fab2), one showed dose-dependent activation of proteolytic activity (Fab3), and two inhibited proteolytic activity (Fab4 and Fab5). We selected our best inhibitory Fab5 (IC_{50} = 722 nM, **Fig. 1.1d**) for further study. Fab5 binds HCMV Pr with a K_d of 1.6 µM as measured by BLI (biolayer interferometry, **Fig. 1.1e**), in good agreement with the measured inhibitory potency.

Fab5 is a Non-Competitive Inhibitor that Isolates HCMV Pr Monomers

HCMV Pr activity is controlled by a conformational transition where multiple discrete events occur to coordinate the active site. Fab5 may inhibit HCMV Pr by occluding the active site or by an indirect mechanism where Fab5 prevents catalytically competent conformations. To evaluate whether Fab5 was a competitive inhibitor, we determined HCMV Pr K_m and V_{max} in the presence of varying concentrations of Fab5 (**Fig. 1.1f**). Increasing concentrations of Fab5 decreases V_{max}, which indicates that Fab5 does not directly compete for substrate binding to the active site. A modest increase in K_m is also observed, possibly indicating the isolation of an HCMV Pr conformation with reduced affinity for substrate binding.

Since dimer formation is vital to HCMV Pr function, we used SEC/MALS (Size-Exclusion Chromatography/Multi-Angle Light Scattering) to determine the stoichiometry of the Fab5/HCMV Pr complex. We combined equimolar amounts of Fab5 and HCMV Pr WT (Wild-Type) and incubated the mixture for 1 hour before injecting the sample. The observed mass of the complex was 78 kDa, which corresponds to one copy of Fab5 (50 kDa) bound to one HCMV Pr monomer (28 kDa) (**Fig. 1.1g**). We also conducted this experiment with HCMV Pr S225M, which carries a mutation that promotes HCMV Pr dimer formation (**Fig.1.1h**). Running HCMV Pr S225M alone results in a single peak corresponding to a HCMV Pr S225M dimer (56 kDa), yet the Fab5/HCMV Pr complex still elutes as a single 78 kDa peak. These results demonstrate that Fab5 isolates and stabilizes HCMV Pr monomers.

Cryo-EM Structure of Fab5/HCMV Pr Complex Reveals a Cryptic Epitope

Fab5 inhibits HCMV Pr by isolating its monomeric state, yet it does not directly block substrate binding. To provide structural insights into how Fab5 isolates HCMV Pr monomers, we used cryo-EM to study the Fab5/HCMV Pr complex. Fab5 and HCMV Pr were incubated at a 1:1 molar ratio, and the stable complex was purified using SEC. We determined the structure of the Fab5/HCMV Pr complex where the entirety of Fab5, including the Fab5/HCMV Pr interface, is resolved to 2.6 Å (**Fig. 1.4a**), which allowed for precise placement of residues of the Fab5 binding site on HCMV Pr, also known as the epitope. The remaining density corresponding to HCMV Pr decreases in resolution with distance from Fab5 due to the flexibility between the two members of the complex.

We determined the sequence of the epitope using *de novo* model building into high-resolution density that did not correspond to Fab5 (**Fig. 1.4b**). We then used lower resolution features of our map to orient the remaining helices and beta-barrel core of one HCMV Pr monomer (**Fig. 1.4c**). The C-terminal region is deleted in our model because we expect this region to be disordered when HCMV Pr is monomeric. A rigid-body placement of HCMV Pr into our map aligns well, which is expected because the globular core of HHV Prs remain intact even when the C-terminal region is disordered.[15] We used AlphaFold3 to generate the initial C-terminal-deleted HCMV Pr model because many loops are missing from HCMV Pr crystal structures. The resulting prediction aligned almost exactly with known structures of HCMV Pr.

Fab5 does not bind near the active site or the dimer interface. Instead, it binds a proline-rich loop of HCMV Pr, which lies between major helices α1 and α2. In dimeric crystal structures, this loop latches the C-terminal tail against the core of the protein (**Fig. 1.4d**), thus we have termed this motif the Latch Loop. Steric hindrance precludes Fab5 from accessing the Latch Loop when HCMV Pr is dimeric, meaning this cryptic site is available when HCMV Pr is a monomer and the C-terminal region is disordered. This leads us to a model (**Fig. 1.4e**) where Fab5 binds to and isolates the HCMV Pr monomer via a conformational selection mechanism.

Fab5 Inhibits HCMV Pr through a Dynamic Allosteric Mechanism

Because Fab5 inhibits HCMV Pr by binding to the Latch Loop and isolating the monomeric state, we hypothesized that the Latch Loop influences the overall conformation of HCMV Pr. In our early reconstructions, we could only resolve the

captured Latch Loop, but then we were able to visualize this flexibility using extensive classification, model building, post-processing via EMReady, and 3D variability analysis (**Fig. 1.5,1.6,1.9**). Four major classes emerge, and HCMV Pr is captured in all classes (**Fig. 1.7a**). Density corresponding to major helices α1 and α2 is resolved in classes One through Three, and we use these features to orient HCMV Pr relative to Fab5. While there is a progressive loss of density furtherer away from the Fab5 interface, lower resolution density corresponding to the beta-barrel and distal helices in classes One and Two leads us to believe that the core of HCMV Pr is still folded similarly to that of known structures. B-factor also decreases distally from the epitope in a linear fashion, indicating a flexible interaction (**Fig. 1.8**).[28] In Class Four, we can see the main epitope of HCMV Pr, but the rest of the protein is unresolved. The Latch Loop acts as a pivot around which HCMV Pr can rock and twist when bound to Fab5 (**Fig. 1.7b**). We hypothesize that classes One, Two, and Three represent energy minima where transient interactions on the Fab5 heavy chain stabilize certain poses of HCMV Pr (**Fig. 1.7c**). For example, residue Y60H (Y60 Heavy chain) on the Fab5 interacts with E122 in Class One (**Fig. 1.7d**) and K119 in Class Two, where K119 can adopt multiple poses (**Fig. 1.7e**). A deeper exploration of epitope plasticity can be found in **Fig. 1.9**. The Latch Loop is a short, fixed 2D epitope. These transient interactions make up a larger plastic epitope that stabilizes a dynamic interaction.

We next examined the structural determinants of how Fab5 prevents dimer formation. We started by placing a hypothetical C-terminal region (purple tube helices, **Fig. 1.7f-h**) alongside our models where we would expect it to be if folded properly. We then docked the composite model into its corresponding EM map and lowered the

threshold. In every case, HCMV Pr becomes enveloped. However, density that would correspond to helices α5 and α6 is not present (**Fig. 1.7f-h** third panels), which suggests that these regions remain disordered. In classes One and Three (**Fig. 1.7f** and **1.7g,** respectively), there is a clash between the heavy chain of Fab5 and the C-terminal tail of HCMVpr. Class Two (**Fig. 1.7g**) is in a pose that could permit proper folding of the C-terminal region, yet there is no EM density to suggest that this happens. Fab5 does not clash with either helix α5 or α6 in any of these poses. Hence, we reason that C-terminal tail displacement is sufficient to disrupt HCMV Pr dimerization through an allosteric mechanism that leads to disorder in the C-terminal region.

The HCMV Pr Latch Motif Governs Dimerization and Activity

Upon closer inspection of the HCMV Pr C-terminal tail in dimeric crystal structures, we noticed that three residues make contacts to hold the tail in place (**Fig. 1.10a**). Residue E122 forms a salt bridge with K255, and Y253 occupies a hydrophobic cleft formed by the Latch Loop while keeping its hydroxyl group solvated. We termed this 3-residue motif the C-terminal Latch Motif, and since Fab5 disrupts the Latch Motif, we wanted to determine its importance in HCMV Pr dimerization and activity. Mutating any of the three latch residues to alanine makes HCMV Pr inactive in a Michaelis-Menten assay (**Fig. 1.10b**), which we carried out at protease concentrations of 0.5 μM. We next evaluated the effect of these alanine point mutations on dimerization by using SEC. HCMV Pr dimer and monomer elute as separate peaks, and we took the ratio of these two peaks at enzyme concentrations ranging from 0.9 μM to 35 μM to determine what percentage of the protease was dimeric (**Fig. 1.10c, 1.11**). Mutants Y253A and

K255A never dimerized in this assay, and E122A could overcome dimer disruption only at the highest concentration of 35 μM. We also measured the thermal stability of the latch mutants using differential scanning fluorimetry. We found that melting temperature decreased only slightly, with K255A having the most significant shift at -3.4°C (**Fig. 1.10d**). From this experiment, we conclude that the latch mutations do not cause HCMV Pr to misfold, and their effects on HCMV Pr activity and dimerization are likely mechanistic. Overall, we establish that the C-terminal latch is a motif with previously unreported importance that can control HCMV Pr activity and dimerization.

Structural and Sequence Conservation of the HCMV Pr Latch Across the HHV Pr Family

There are nine human herpesviruses classified into three subfamilies (α, β, and γ) (**Fig. 1.12a**), and the structures of 6 HHV Prs have been solved. HCMV Pr, a β herpesvirus, has a sequence similarity of 24-38% to other HHVs, yet the other known HHV Pr structures share its fold, dimeric state, and active site residues. The C-terminal latch is one of the few conserved motifs across the HHV Prs. HCMV Pr shares identical latch motif residues with all members of the β and γ herpesviruses, and while the latch sequences of the α herpesviruses diverge, there is structural conservation in this region. We wanted to assess whether the latch motif is as important in other HHV Prs as it is in HCMV Pr, so we made alanine mutations in Kaposi's sarcoma-associated virus (KSHV) and Eppstein-Barr virus (EBV), which are both γ herpesviruses (**Fig. 1.12b**). Mutating the latch residues in KSHV also inactivate the enzyme in a Michaelis-Menten activity assay (**Fig. 1.12c**)

Discussion

Dimerization of HHV Prs triggers conformational rearrangements that coordinate the active site and lead to catalytic competency. These structural constraints, combined with the fact that HHV Prs are expressed as Pr-AP fusions, exert spatial and temporal control to minimize activation of the Pr domain before it reaches the interior of a viral capsid. We identified a conformationally selective inhibitory Fab termed Fab5 which inhibits HCMV Pr by isolating its monomeric state. Cryo-EM structures of the Fab5/HCMV Pr complex reveal a short proline-rich epitope that is distal from both the interfacial helix α5 and the oxyanion loop-stabilizing helix α6, as well as the active site. In dimeric HCMV Pr crystal structures, the Fab5 epitope typically pins the C-terminal tail to the core of the protein, which led to us referring to the epitope as the Latch Loop. HCMV Pr has a large range of motion when bound to Fab5, which we visualized by resolving 3 unique binding poses from a single cryo-EM dataset. Two of these states clash with a hypothetical folded C-terminal tail in the active dimeric conformation, which led us to hypothesize that Fab5 disrupts the dimer interface through both steric hindrance and the sequestration of an important binding loop in the HCMV Pr conformational cycle. In crystal structures, E122 on the Latch Loop forms a salt bridge with K255 on the C-terminal tail, and Y253 is enveloped by this interaction. An alanine scan of this E-Y-K Latch motif demonstrated that these residues play an important role in both dimerization and proteolytic activity. Because all HHV Prs have a Latch Loop and two-thirds of HHV Prs share the same latch motif as HCMV Pr, the Fab5 mechanism of inhibition represents a new route to HHV Pr inactivation by targeting a cryptic allosteric site.

13

The sequences of all HHV Pr Latch Loops also contain multiple proline residues. Proline-rich motifs (PRMs) often preclude visualization by structural biology because they seldom participate in secondary structure. While PRMs are disordered in this sense, proline does increase the order of loops by constraining the conformational space of neighboring residues. The result is a rigidified amino-acid backbone, which lowers the entropic cost of binding, which is why PRMs often participate in protein-protein interaction (PPI). In a host cell, the HHV Pr domain is also linked to an AP domain, which itself contains 12.8% proline. The AP is also composed primarily of alanine and serine, which, together with proline, comprise 44.7% of its sequence. Pr-AP fusions likely aggregate through PRM interactions with loosely defined quaternary structures and ultimately form a spherical procapsid together with the major capsid protein (MCP). Once concentrated inside the procapsid, the Pr domain relies on a PRM via the Latch Loop to assume its active form, and Fab5 exploits this interaction to inhibit activity.

Fab5 exhibits a mechanistic example of allostery where Fab5 binding leads to the disorder of discrete conformational elements, such as helix α6, that are required for catalytic competency. However, it is also possible that conformational entropy redistribution plays a role in the way Fab5 disrupts active site coordination. We recently provided comprehensive evidence linking cryo-EM density loss and B-factor changes to conformational flexibility and entropy redistribution in protein complexes. Namely, rigidification of a protein interface can lead to increased flexibility in distal areas. Molecular dynamics studies of homologous KSHV and Varicella Zoster (VZV) Prs corroborate this model by indicating that dimerization induces lower conformational

mobility at the dimer interface and increases mobility at the substrate binding pocket.[29] In addition to disrupting the interaction between the Latch Loop and the C-terminal tail, Fab5 binding may introduce flexibility in both the active site and the start of the C-terminal region. Both sites are antipodal to the Latch Loop, and we observe the total loss of density corresponding to the oxyanion loop and the entire C-terminus and drastic increases in B-factor. While Fab5 displaces the C-terminal tail in classes One and Three, Class Two could permit proper folding of the dimer interface. Fab5 binding may introduce greater overall flexibility into the C-terminal region which, in addition to Latch Loop binding, results in an entropic barrier to dimer interface formation that is too high for HCMV Pr to overcome.

The dynamic network that links HHV Pr dimerization to activity is well-established and complex and ultimately results in a dearth of stable surfaces on the Pr domain,[9,13] which is likely why the primary epitope of Fab5 is only seven residues in length. Despite the flexibility between Fab5 and HCMV Pr, we believe our 3 atomic models represent energy minima in the motion of HCMV Pr that provide a framework for improving the affinity of Fab5. By creating a phage-displayed sub-library with mutations in the complementarity determining regions (CDRs) of the Fab5 heavy chain, a panning campaign could result in new binders that stably capture more distal residues on HCMV Pr like W179 and R183. Interactions such as this could transform an ultimately two-dimensional epitope into a true three-dimensional one. Furthermore, the propensity of Fab5 for PRM binding could mean that Fab5-based sub-libraries are a feasible starting point to isolate Fabs against homologous HHV Prs.

In this work, we harnessed the synergy between antibodies and cryo-EM as the foundation to characterize a loop in HCMV Pr with broader implications for therapeutic development across the HHV Pr family. Our efforts also establish a framework for Fab epitope mapping via cryo-EM which enables structure-guided study and design of antibodies. From the perspective of cryo-EM, the asymmetric Fab5/HCMV Pr complex is small and flexible,[30] which poses a technical challenge to structure determination. We, among others,[31] demonstrate that there should be no size or flexibility limitations on antigens when mapping the epitope of a Fab via cryo-EM using currently available technology.
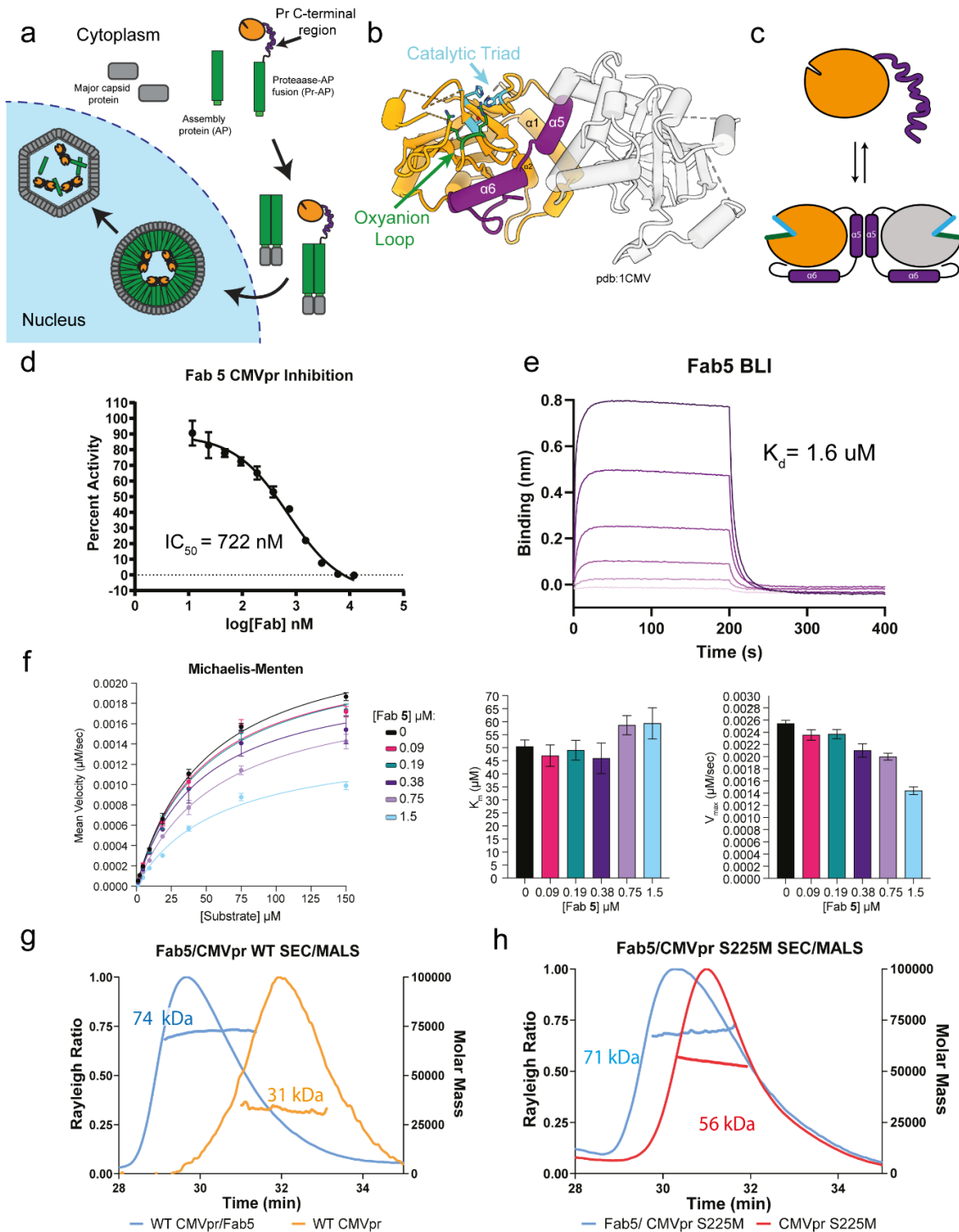
Figures

Figure 1.1: The HCMV Pr conformational cycle and characterization of Fab5 a) HCMV Pr is expressed as a fusion with the assembly protein (AP) in the host cytosol. It then traffics into the nucleus where the complex incorporates into maturing (figure caption continued on next page)

17

(figure caption continued from the previous page)viral capsids. The Pr domain dimerizes in the capsid and becomes active, and then frees both itself and AP from the major capsid proteins, allowing for viral capsid maturation. b) Crystal structure of HCMV Pr dimer showing catalytic triad (blue), oxyanion loop (green), and C-terminal region (purple) comprised of helices α5 which forms the dimer interface, and α6 which stabilizes the oxyanion loop. c) Disorder-to-order transition of the HCMV Pr domain. d) Fab5 inhibits HCMV Pr with an IC_{50} of 722 nM. e) Fab5 has a K_d of 1.6 μM. f) The Michaelis-Menten curve of HCMV Pr was determined in the presence of varying concentrations of Fab 5 (left). The K_m and V_{max} were quantified for each Fab 5 concentration and are summarized as bar graphs (right). Data are reported from triplicate technical replicates as the mean ± standard deviation (Michaelis-Menten) or standard error of mean (K_m, V_{max}). g) Fab5 isolates a monomer of both WT HCMV Pr (g) and the dimer-promoting mutant S225M HCMV Pr (h) determined via SEC-MALS.
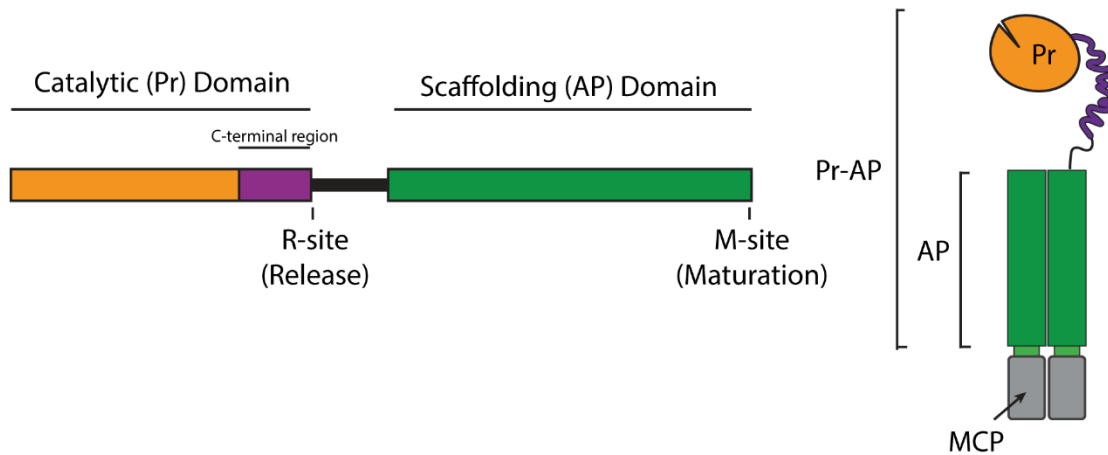
Figure 1.2: Schematic of the UL80 gene The HCMV UL80 gene. Primary components are the catalytic domain, a linker region, and the Scaffolding domain. Proteins can either be expressed as Pr-AP or AP due to multiple open reading frames. Pr-AP associates with the major capsid protein (MCP) in the cytosol. Catalytically competent Pr frees itself from AP via the R-site, and the scaffolding is cleared away via the M-site. The wild-type Pr domain contains multiple autoproteolytic sites, which is why our expression construct contains mutations (A141V, A143V, P144A and A209V) to limit autoproteolysis.

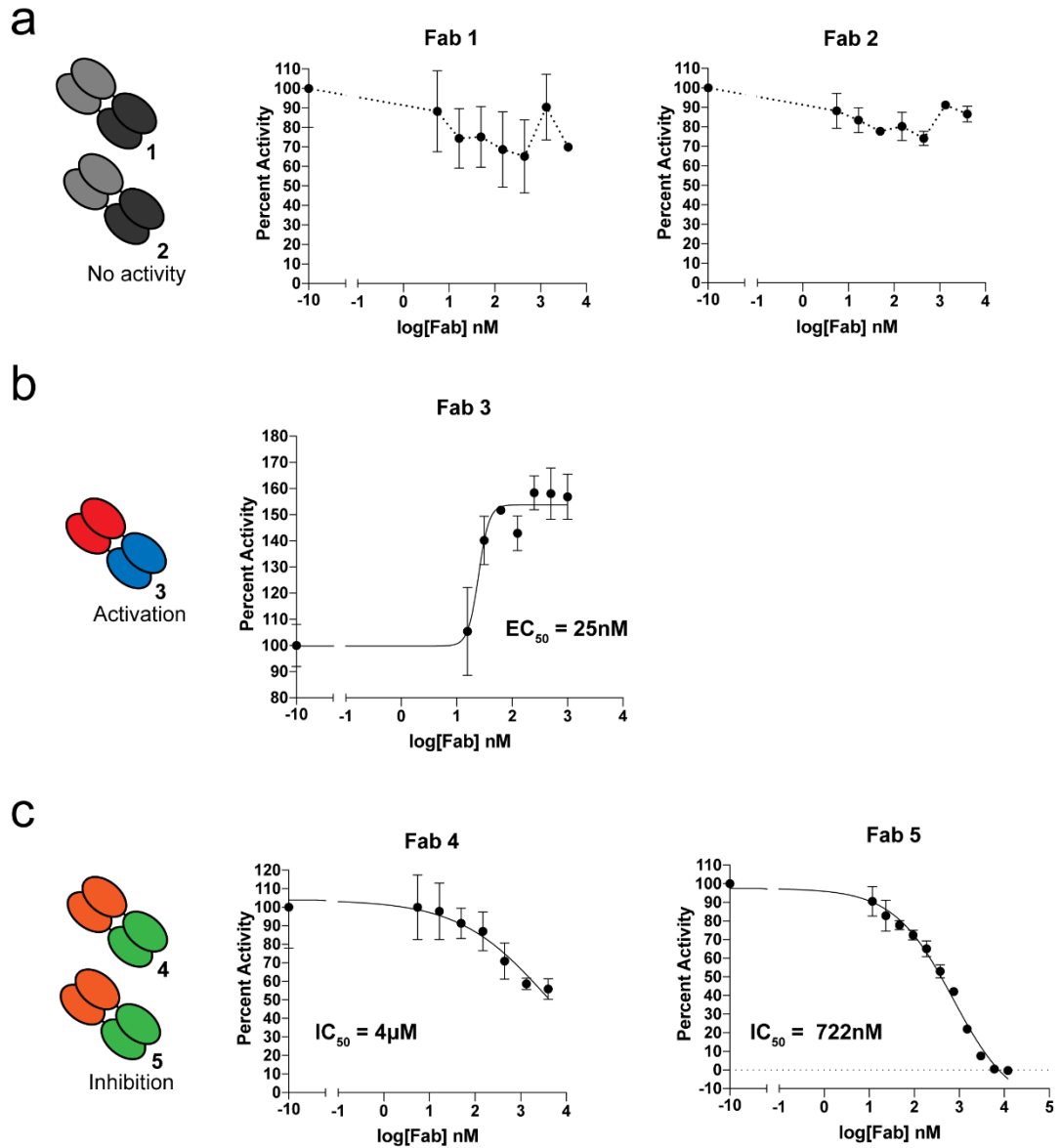**Figure 1.3: Inhibition assay with 5 unique Fab clones** Inhibition assay with the five unique clones from HCMV Pr phage-displayed panning. Fab5 has the best IC50. We did attempt to carry forward with study of Fab3 (an activator) as well, but we were not able to purify a stable complex on SEC or visualize a complex via negative-stain EM
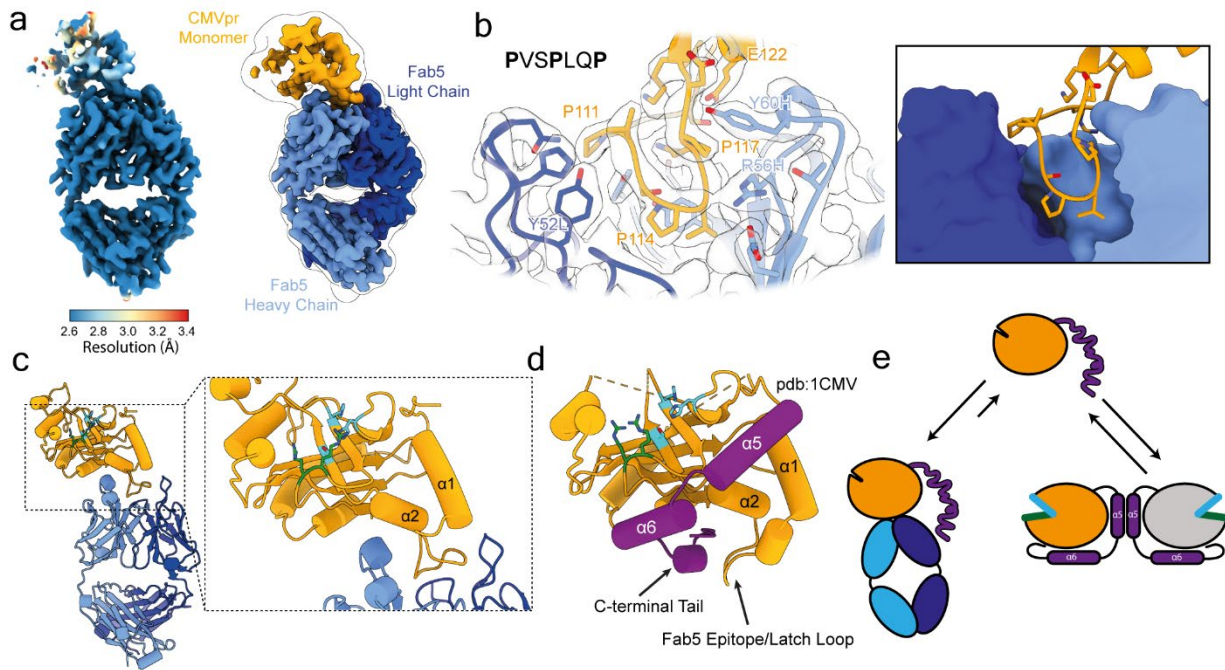
Figure 1.4: Cryo-EM reveals Fab5 epitope a) cryo-EM structure of the Fab5/CMVpr complex at a resolution of 2.6 Å. b) Model of the Fab5/HCMV Pr interface docked into EM density (left). The sequence of the captured loop is written in black, and key residues are labeled. The Fab5 epitope extends deep between the Fab5 heavy and light chains (right). c) Model of Fab5/HCMV Pr complex showing that Fab5 binds distally from the active site (cyan and green residues). d) Fab5 epitope, or Latch Loop, marked on a dimeric crystal structure of HCMV Pr (one monomer shown). e) Fab5 isolates monomeric states of HCMV Pr.
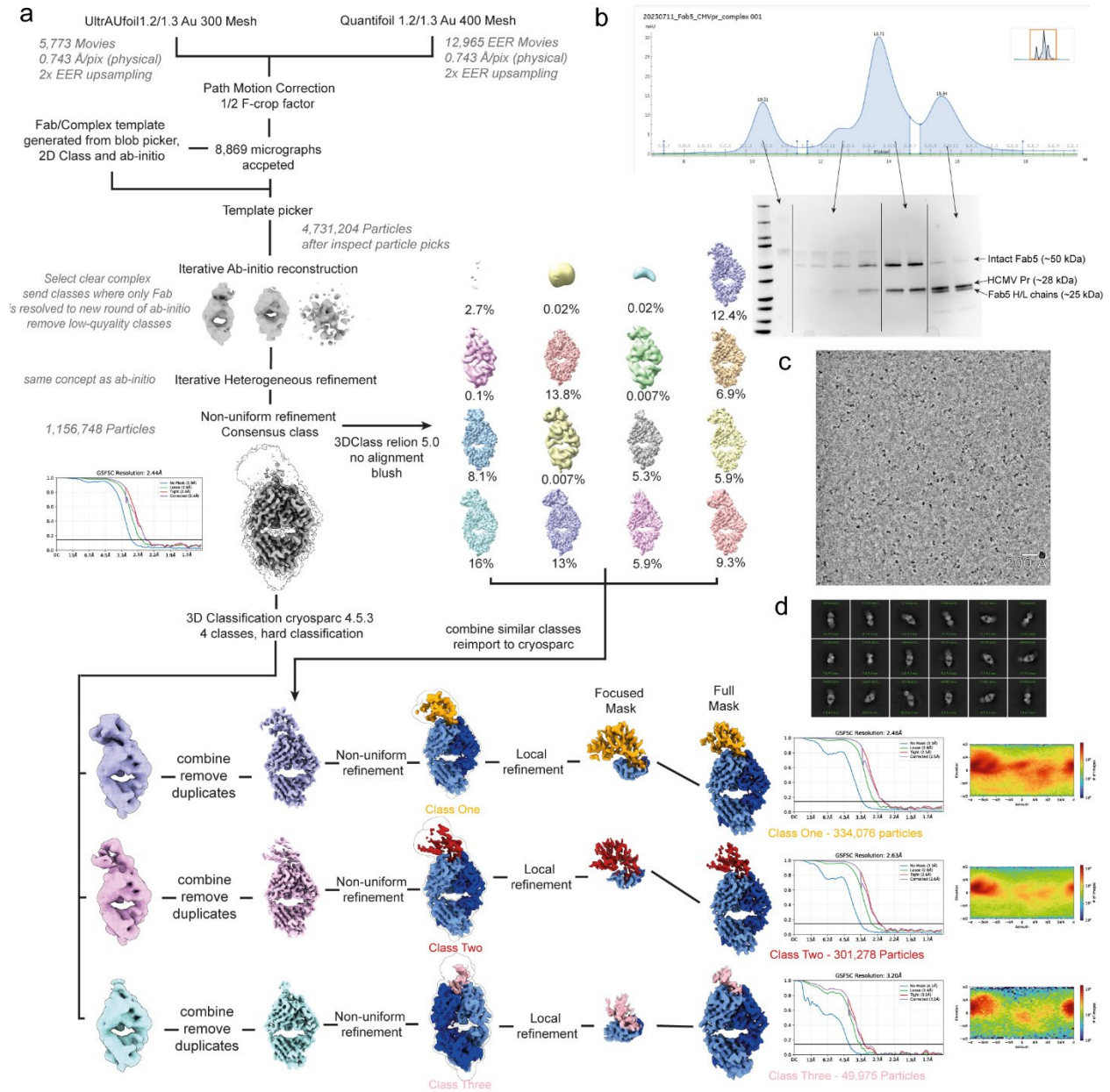
Figure 1.5: Flow chart of EM data processing a) Flow chart of EM processing workflow. The graphs next to the final volumes in the bottom right are GSFSC curves and orientation distributions for final volumes. Final volumes for classes One, Two, and Three were solved using non-uniform refinement, local refinement with a focused mask, and local refinement with a full mask. All volumes were used iteratively for model building. b) size-exclusion chromatography of Fab5/HCMV Pr complex preparation. Only the largest peak was used for cryo-EM sample. c) Representative micrograph of Fab5/HCMV Pr complex. d) representative 2D classes of Fab5/HCMV Pr complex.
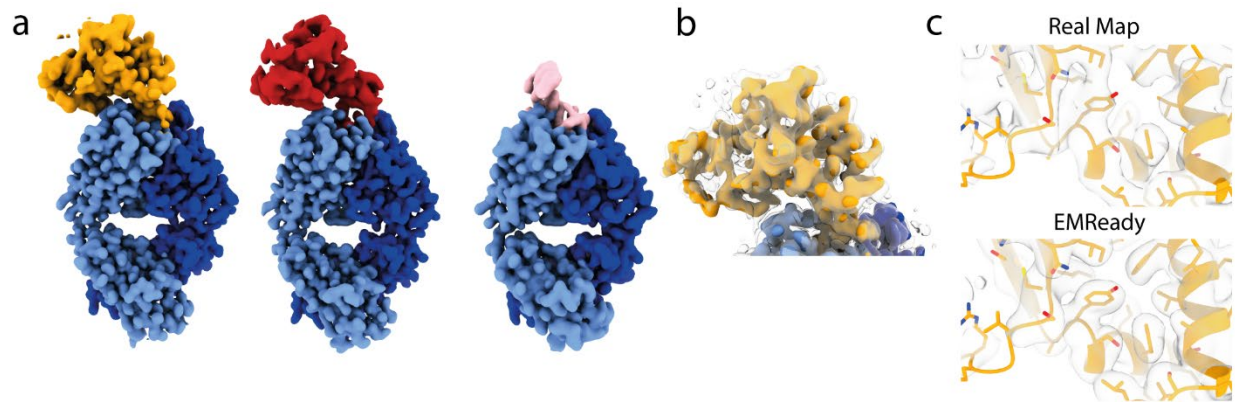
Figure 1.6: Map comparison with EMReady a) EMReady post-processing results of final maps for classes One (orange HCMV Pr), Two (Red) and Three (pink). b) Transparent real map overlayed with EMReady map for Class One. c) Representative comparison of side-chain density between real maps and EMReady maps. All models built using an EMReady improved map were manually checked against real maps and were also validated using Phenix Comprehensive Validation against real maps.
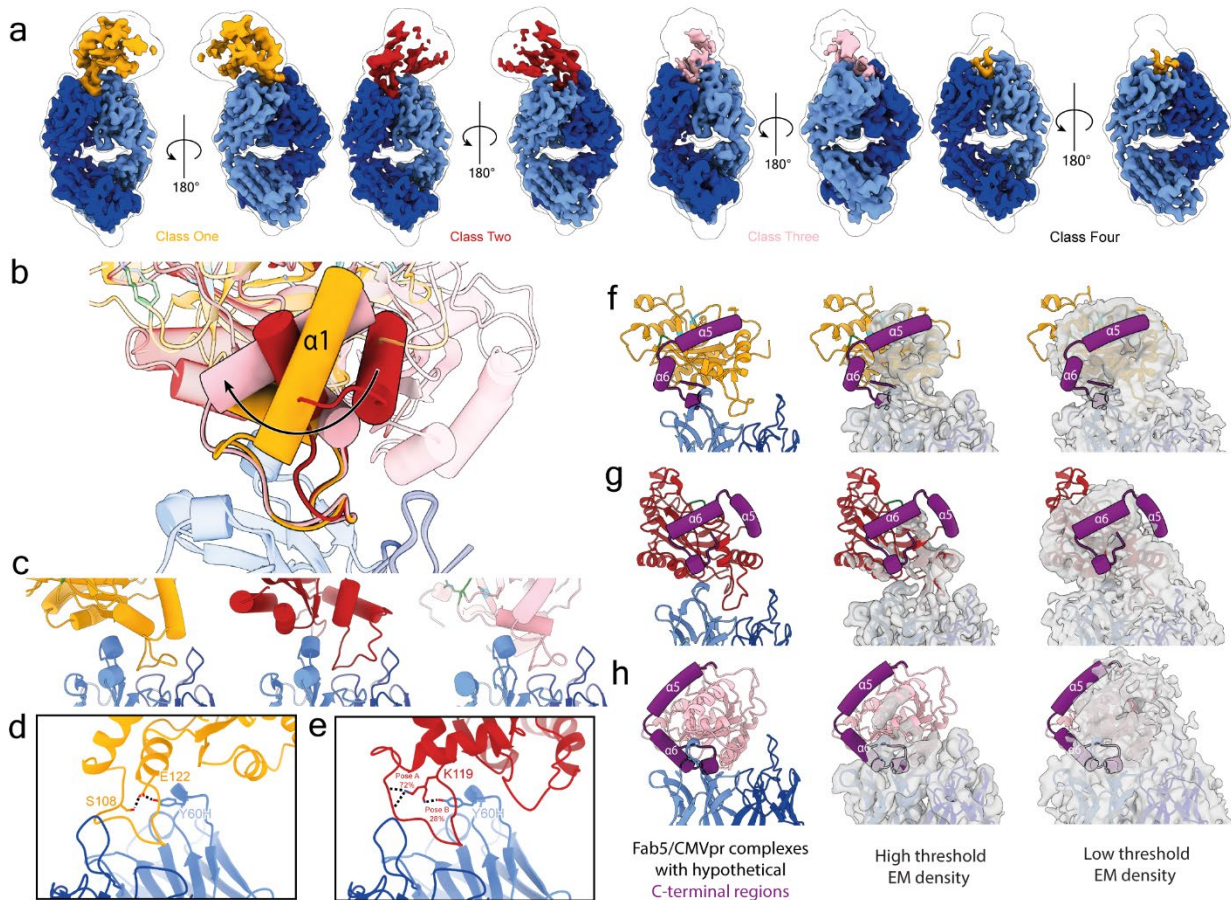
Figure 1.7: Multiple states of HCMV Pr all show C-terminal disorder a) Major classes from 3D classification show that HCMV Pr is flexible when bound to Fab5. b) Models of classes One (orange), Two (red), and Three (pink) superimposed. Focusing on helix α1, twisting and rocking motions of HCMV Pr can be observed. c) Transient contacts are made between the Fab5 heavy chain (light blue) and the various poses of HCMV Pr, demonstrating the plasticity of the overall epitope. d) Fab5 residue Y60H makes a predicted hydrogen bond (black dashed line) with HCMV Pr residue E122 in Class One. e) In Class Two, Y60H interacts with K119. K119 can adopt alternate poses, interacting either with Y60H or the HCMV Pr Latch Loop. f-h) Models of Fab5/HCMV Pr complex with folded C-terminal region from an intact HCMV Pr dimer superimposed. The models are then fit into EM density with high and low thresholds. Fab5 clashes with the C-terminal tail in Class One (f), and there is no density that would correspond to a folded C-terminal region. Class Two could permit the C-terminal region to fold (g). However, density for this region is still not observed. Class Three (h) clashes with the C-terminal region as well.
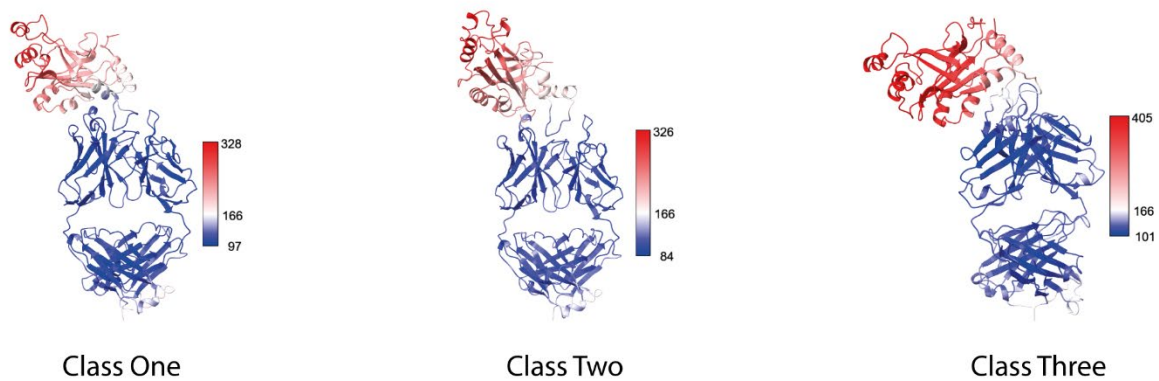
Figure 1.8: B-factor mapped onto Fab5/HCMV Pr models Fab5/HCMV Pr complexes colored by B-factor. B-factor was calculated with Phenix Real-Space Refinement. B-factor at the interface is about the same as the entirety of the Fab in each model and increases on HCMV Pr with greater distance from the epitope.
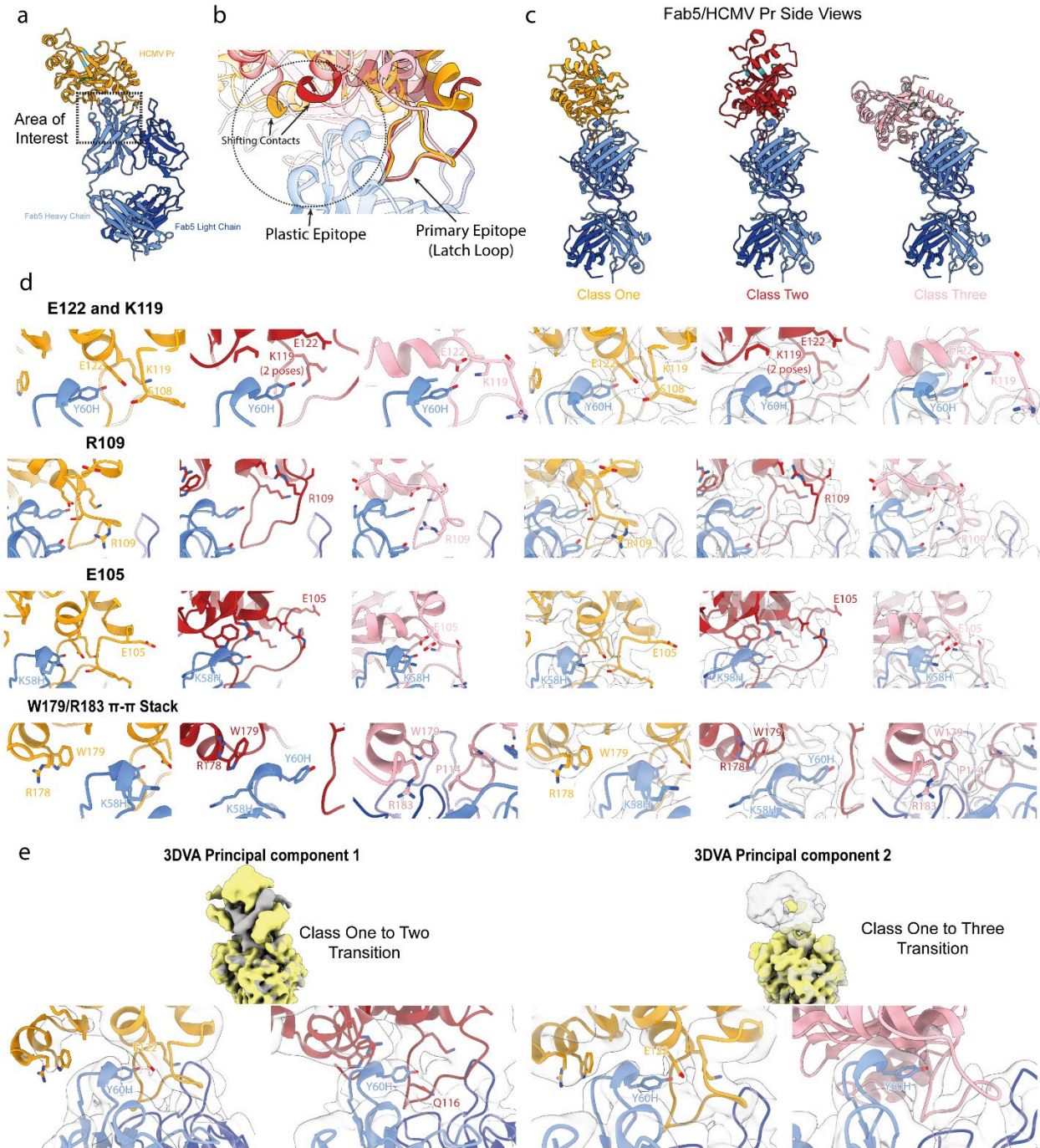
Figure 1.9: Exploration of Fab5 epitope plasticity a) model of Class One for reference to area of interest. b) The area over the Fab5 heavy chain is circled. We call this area the plastic epitope because transient contacts form here in the different Classes. The movement of a short helix is highlighted. On the right, the primary epitope is highlighted. Residues caught between the Fab5 heavy and light chains align well between classes, then rapidly diverge distally from the Fab. c) Side views of models for reference of HCMV Pr motion. d) Vignettes of shifting contacts between classes. First three frames are inter-class comparisons, last three frames are the same image with EM volume superimposed. **E122 and K119** in Class One, (figure caption continued on next page)

(figure caption continued from the previous page) E122 is engaged by both Y60H and S108. In Class Two, E122 is peeled away from the interface and Y60H engages K119 instead. K119 can adopt multiple poses, and occupies density near Y60H about 25% of the time. E122 comes back into contact with Y60H in Class Three, however density is weak. S108 now points towards solvent. **R109** In both Classes One and Two, density for R109 is weak and it points towards solvent. R109 adopts multiple poses in Class One, pointing mostly towards solvent. Class Three has the strongest density for R109 as it lays across the top of the Fab5 heavy chain. **E105** is similar to R109 insofar as it points towards solvent in Classes One and Two while making interactions, albeit weakly, with K58H in Class 3. **W179 and R183** make a pi-pi stack between their respective indole ring and guanidino group. In Class One, the pair pack against the Fab5 heavy chain more distally from the interface, whereas in Class Two they pack above K58H, closer to the interface. In Class Three, the pi-pi stack is broken, and the W/R residue pair is smeared near the primary epitope. This pair of residues completes an arc of about 30 angstroms in length between the three classes. e) 3D Variability analysis was run with five principle components with all particles from all three classes. Two scenes are highlighted where Y60H can be observed changing contacts as HCMV Pr twists and rocks on Fab5.
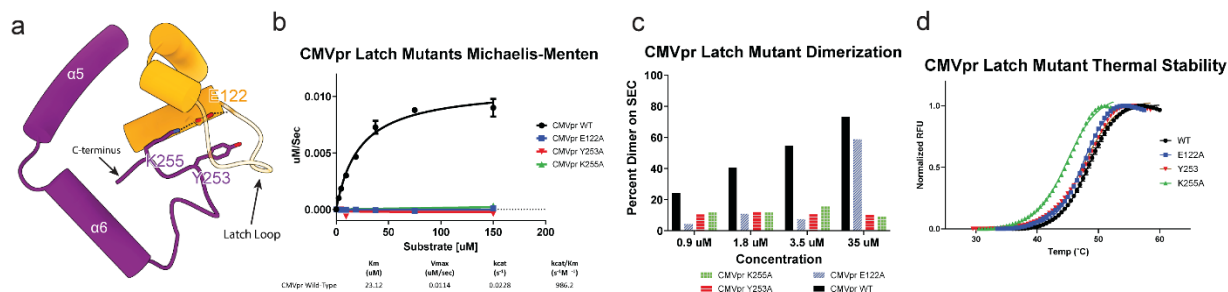
Figure 1.10: Mutagenesis of the Latch Motif in HCMV Pr a) The Latch Motif, comprised of E122 on the HCMV Pr Latch Loop and Y253 and K255 on the C-terminal tail. b) Mutating any of the Latch Motif residues to alanine results in no activity in a Michaelis-Menten assay. c) Latch Motif mutants disrupt dimerization. Percent dimer is calculated by integrating the peak area of monomer and dimer HCMV Pr peaks on SEC, then plotting the ratio. WT HCMV Pr dimerizes in a concentration-dependent manner, and the Latch mutants remain in monomeric states. Only E122A is able to overcome dimer disruption at the highest concentration measured. d) Thermal stability measured via DSF. Latch mutants have small melting temperature shifts, suggesting that these mutations do not cause HCMV Pr to be misfolded.
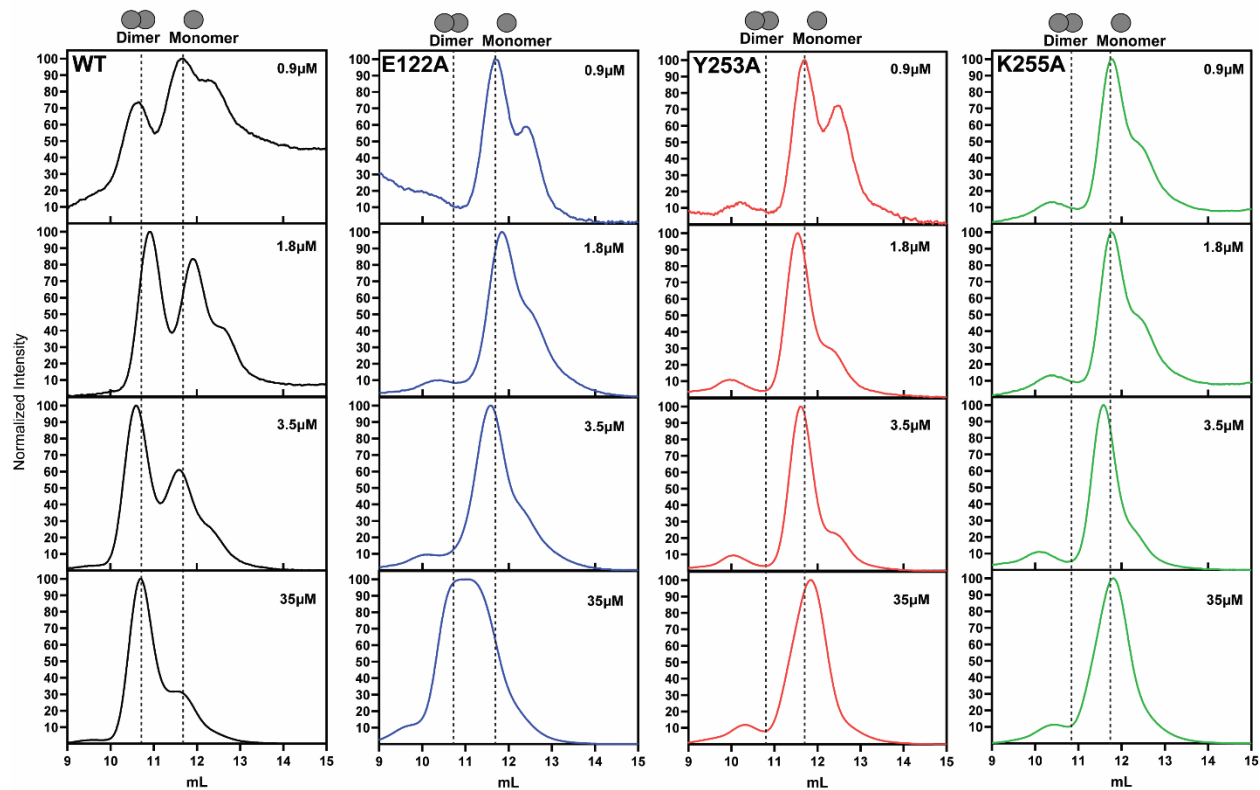
Figure 1.11: SEC chromatograms of dimer formation All SEC chromatograms from dimerization experiments. Peak areas were integrated, and a ratio was taken to make the percent dimer graph in Fig. 4. Results are normalized for intensity, and the x-axis has column volume. The left column is wild-type HCMV Pr, and concentration-dependent dimerization can be observed. All mutant constructs remain as monomers except for E122A, which can dimerize at the highest concentration.
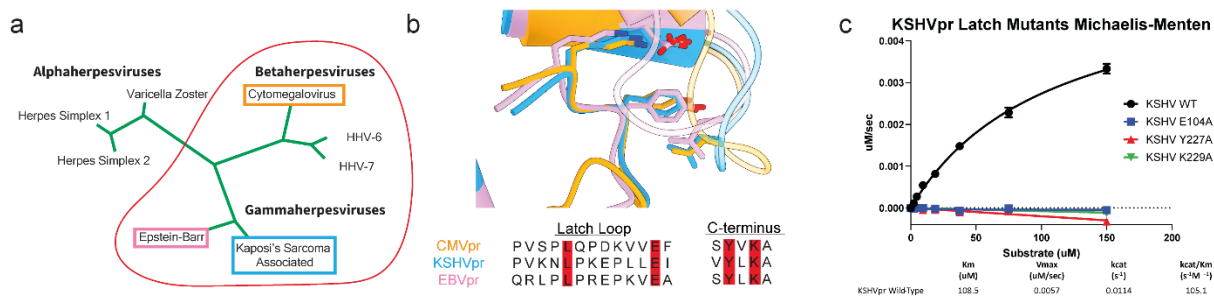
Figure 1.12: Conservation of the Latch Motif across HHV Prs a) Phylogenetic tree of the human herpesvirus family. The red circle indicates which HHV Prs have a conserved Latch Motif. b) Structural and sequence alignment of HCMV Pr, KSHV Pr, and EBV Pr. The Latch Loop in all three Prs is rich in proline and the critical glutamate residue in the Latch Motif is conserved, along with lysine and tyrosine residues at the C-terminus. A leucine that packs together with the tyrosine is also conserved. c) Mutating Latch Motif residues on KSHV Pr also disrupts activity in a Michaelis-Menten assay.

Materials and Methods

Phage display panning: A fully human naïve B cell Fab library was displayed on phage. Antigen was biotinylated using EZ-Link NHS-Chromogenic-Biotin (Pierce), immobilized using magnetic streptavidin beads (Invitrogen) and underwent four rounds of selection with decreasing concentration of antigen. Candidate Fabs were identified using dotblots and subsequently expressed, purified and validated using biolayer interferometry.

Fab expression and purification: Fabs **1-5** were expressed and purified as previously described.[27]

HCMV Pr Mutagenesis: All HCMV Pr constructs bear a N-terminal 6X-His tag. Point mutagenesis was performed using a Quickchange Lightning Site Directed Mutagenesis Kit (Agilent). PCR products were transformed into XL-10 Gold competent *E. coli* cells and selected using Ampicillin (AMP) and Chloramphenicol (CAM). Cultures were grown in 5 mL Luria Broth (LB) supplemented with AMP (100 µg/mL final concentration) and CAM (34 µg/mL final concentration) while shaking at 37°C overnight. DNA was isolated using a Qiagen Miniprep Kit and sequenced.

HCMV Pr Expression: HCMV Pr constructs were expressed in Rosetta 2 BL21 *E. coli* cells (Millipore). Cells were grown in 50 mL LB supplemented with AMP (100 µg/mL) and CAM (34 µg/mL) while shaking at 37°C overnight. The next day, 10-50 mL of culture was used to inoculate 1 L LB supplanted with antibiotics and shaken at 37°C to an

OD$_{600}$ of 0.6. Isopropyl β-d-1-thiogalactopyranoside (IPTG) was added (1 mM final concentration) and cultures were shaken at 16°C overnight.

HCMV Pr Purification: Cells were harvested, pelleted and suspended in a buffer containing 50 mM potassium phosphate at pH 8.0, 300 mM KCl, 25 mM imidazole and 5 mM 2-mercaptoethanol (BME). Cells were lysed by microfluidization and pelleted, and the supernatant was purified on a GE HealthCare LifeSciences Akta Explorer FPLC at 4°C. Protein was eluted over two stacked 5 mL HisTrap Nickel columns with gradient elution into a buffer containing 25 mM potassium phosphate at pH 8.0, 150 mM KCl, 300 mM imidazole and 5 mM BME. Eluate was collected and dialyzed overnight against a buffer containing 25 mM potassium phosphate at pH 8.0, 150 mM KCl, 0.1 mM EDTA and 1 mM BME. Dialyzed protein was concentrated to ~2 mL and purified over HiLoad 26/60 Superdex 75 (GE Healthcare) into the same buffer. Protein bands were analyzed by SDS-PAGE and pure protein was collected, flash frozen and stored at -80°C. Protein concentrations were determined using a NanoDrop 2000c UV spectrophotometer (Thermo Scientific) using an extinction coefficient of 28,420 M^{-1} cm^{-1} for all HCMV Pr constructs.

Michaelis-Menten Kinetics: HCMV Pr, KSHV Pr, and their respective Latch Motif mutants were diluted to 500 nM in buffer containing 25 mM potassium phosphate at pH 8.0, 150 mM KCl, 0.1 mM EDTA, 1 mM BME , 10% glycerol and 0.01% TWEEN-20. An internally quenched FRET substrate was used: NH$_2$-Lys(MCA)-Tbg-Tbg-Asn-Ala-Ser-Ser-Arg-Leu-Lys(Dnp)-Arg-OH, where Tbg is L-*tert*-leucine, Lys(MCA) is a lysine

residue with side chain linked to a 7-methoxycoumarin-4-acetic acid and Lys(Dnp) is a lysine linked to 2,4-dinitrophenyl. Substrate was prepared in 1:2 serial dilutions from 7.5 – 0.06 mM in DMSO, then 98µL protein + 2 µL substrate (150 – 0.3 µM final concentration) in a 96-well black untreated polystyrene plate. Enzyme velocity was monitored by fluorescence increase (excitation: 328 nm, emission: 393 nm) on a BioTek Synergy H4 Bioreader at 30°C. Mean velocity (RFU/s) during steady state was fit using BioTek Gen5 data analysis software. The mean velocity of control wells containing only buffer and substrate was averaged and subtracted from calculated enzyme velocity. A serial dilution of free MCA was prepared, ex/em at 30°C was determined and fluorescence (RFU) was plot in triplicate against MCA concentration (µM) then fit to a linear regression to get a slope of 11053 RFU/µM, which was used to convert initial velocity values from RFU/s to µM/s. Substrate concentration vs. velocity curves were plot in GraphPad Prism then fit using the standard Michaelis-Menten and k_{cat} equations then resulting values were used to calculate k_{cat}/K_m with standard propagation of error. All data were collected duplicate or triplicate from technical replicates and are reported in figures as the mean, including error bars depicting standard deviation.

IC$_{50}$ values: *Panning hit validation*: HCMV Pr was diluted to 1 µM in buffer containing 25 mM potassium phosphate at pH 8.0, 150 mM KCl, 0.1 mM EDTA and 10% glycerol. Fab **1**, **2**, **3**, **4** or **5** was diluted in 1:3 serial dilution from 8 - 0 µM in phosphate-buffered saline (PBS) then 48 µL HCMV Pr solution and 50 µL Fab solution was combined in a 96-well black untreated polystyrene plate and incubated for 20 min at room temperature (500 nM HCMV Pr final, 5% glycerol). A 7-amino-4-carbamoylmethylcoumarin (ACC)

cleavable substrate was used: Ac-NH-Tbg-Tbg-N4Me$_2$Asn-Ala-ACC, where Ac-NH refers to an acyl capped N-terminus, Tbg is L-*tert*-Leucine and N4Me$_2$Asn is N4,N4-dimethyl asparagine. Substrate diluted in DMSO was added to the HCMV Pr + Fab solution (2 µL, 40 µM final) and enzyme velocity was monitored by fluorescence increase (excitation: 380 nm, emission: 460 nm) on a BioTek Synergy H4 Bioreader at 30°C. The velocity (V) of PBS-only controls was averaged and used to normalize data as percent activity:

$$\%\text{Activity} = \left(\frac{V_{\text{compound}}}{V_{\text{DMSO}}}\right) \times 100$$

The log$_{10}$[Fab] was plotted vs. percent activity and curves were fit with a standard four parameter log(inhibitor) vs. response with variable hill slope equation.

Biolayer-interferometry: Fab **5** was diluted into PBS then biotinylated for 1 h at room temperature using EZ-Link NHS-Chromogenic-Biotin (Pierce).[27] HCMV Pr, HCMV M75A or HCMV R79A was dialyzed into buffer containing 25 mM potassium phosphate at pH 8.0, 150 mM KCl and 0.1 mM EDTA then diluted to 50, 500 or 5000 nM in the above phosphate buffer plus 1% bovine serum albumin and 0.01% TWEEN-20. Biotinylated Fab **5** was immobilized on ForteBio streptavidin SA biosensors and the affinity of each HCMV Pr construct for Fab **5** was determined on an Octet RED384 biolayer interferometer as previously described.[27]

Size-exclusion chromatography and multi-angle light scattering: *HCMV Pr + Fab 5:* Equimolar amounts of Fab 5 and HCMV Pr were mixed and incubated at room temperature for 1 h. 500 µL of the mixture was injected onto a Superdex75 10/300

column and eluted over 1 CV. Low molecular weight standard (source) was injected onto the same column and eluted in the same buffer at the same flow rate. Linear regression analysis of the elution peaks using R allowed interpolation of the apparent molecular weight of the complex.

HCMV Pr dimerization: WT HCMV Pr, HCMV M75A or HCMV F155A were diluted (0.9 µM, 1.8 µM, 3.5 µM or 35 µM final concentration) into buffer containing 25 mM potassium phosphate pH 8.0, 150 mM KCl, 0.1 mM EDTA, 10% glycerol and 1 mM β-mercaptoethanol then incubated at room temperature for 1-7 h. A Superdex 75 10/300 GL column was equilibrated at 4°C into the same buffer used to dilute proteins. For all protein samples, 500 µL was injected onto the column and protein eluted over 1 CV at 0.6 mL/min flow rate while monitoring Absorbance at 280nm. For each individual sample run, the absorbance at A280 was plotted against time (min). The minimum absorbance value across the full spectrum was calculated in Microsoft Excel and subtracted from each absorbance value to correct the baseline to zero. The maximum absorbance between 14-23 min was calculated, then all data were normalized to this value using the following equation, where A_x is the 280 nm absorbance at time x and A_{max} is the maximum value calculated between 14-23 min:

$$Normalized\ Intensity = \left(\frac{A_x}{A_{max}}\right) \times 100$$

Multi-angle light scattering was performed by running the elution from an SEC run and injecting into a Wyatt Dawn Pro and Optilab combined instrument. Data were plotted in Astra and imported to GraphPad Prism where they were overlayed on normalized SEC data using a second Y-axis.

Cryo-EM Sample Preparation and Data Collection: Fab5/HCMV Pr complex was purified by SEC and concentrated to 1 mg/mL. The sample was diluted to 0.1 mg/mL and 3 microliters was pipetted onto glow-discharged gold grids coated in holey carbon film (Quantifoil, 300 mesh 1.2/1.3, Au) or holey gold film (UltrAuFoil, 400, mesh 1.2/1.3). Grids were then blotted and plunge-frozen using a Vitrobot Mark IV equipped with Whatman type 4 blotting paper with a blotting time of 4 s and blotting force of -2, at 4 °C and 100% humidity. Data was collected at the Janelia Research Campus in Ashburn, VA on Krios 3. This 300 keV microscope is equipped with a Thermo Scientific Falcon 4i camera, Selectris X energy filter, and cold Field emission gun with 6 eV slit width during acquisition. A nominal magnification of 165,000x was used for a physical pixel size of 0.743 (0.371 in super resolution) with a total dose of 50 e-/A˚2. Automated data collection was performed using SerialEM to collect movies with a defocus range between 0.8-2.0 A˚.

Image Processing: Dose-fractionated super resolution images stacks were motion corrected and Fourier-cropped by 2 using both cryoSPARC and MotionCor2. CTF estimation was performed using cryoSPARC, followed by micrograph curation, blob-based particle picking, 2D classification, and ab initio modeling. The *ab initio* model was used to generate templates for further particle picking and curation. Iterative rounds of multi-class *ab initio* modeling and heterogeneous refinement were used to generate particle stacks where HCMV Pr could be resolved in the complex. Particles were then sent to Relion using the PyEM code suite for 3D Classification. Particles were then reimported to cryoSPARC for further 3D Classification, reference-based motion correction, 3D refinement, and 3D variability analysis.

Model Building and Refinement: A model of Fab5 generated by Alphafold 3 was docked into cryo-EM density and refined using ISOLDE and PHENIX. To identify the Fab5 epitope, we generated each flexible loop of HCMV Pr as a peptide in COOT and began modeling it into the non-Fab5 cryo-EM density. We identified that the loop from P111-P117 fit this density well, and then appended the rest of an HCMV Pr monomer onto it (PDB:1CMV) and built the missing loops in COOT. The complete model was further refined using real-space refinement in PHENIX and ISOLDE. Cryo-EM maps enhanced with EMReady were also used in intermediate stages of the modeling process. B-factors were calculated in PHENIX.

Chapter 2

X-ray Footprinting Reveals HCMV Pr Allosteric Network

Abstract

X-ray footprinting and mass spectrometry (XFMS) is a way to assess the solvent accessibility of individual amino acid residues in solvent. By performing XFMS on the Fab5/HCMV Pr complex, we corroborate our model that Fab5 isolates HCMV Pr monomers by binding to the Latch Loop. We also observed that certain residues around the active site, namely M75, are protected from solvent when Fab5 binds HCMV Pr. Because we do not resolve M75 or most of the active site in our cryo-EM structures, we employed a multipronged approach using HSQC NMR, mutagenesis and biochemical assays to investigate the importance of M75 and surrounding residues on HCMV Pr activity and dimerization. We discovered that M75 is part of an allosteric network together with F155 that is conserved across the HHV Pr family and plays a key role in activity and dimerization.

Introduction

Fab5 is a conformationally selective antibody that inhibits human cytomegalovirus protease (HCMV Pr) by isolating its monomeric state. HCMV Pr is a dynamic protein that changes conformation between monomeric and dimeric states, and as we show in our cryo-EM structures, the interaction between Fab5 and HCMV Pr is also dynamic. Three-dimensional structures are ultimately static snapshots of a structural landscape. While new methods in cryo-EM are enabling the interpretation of protein dynamics,[28] we are interested in elucidating the dynamics of HCMV Pr and the Fab5/HCMV Pr complex in solution. We used X-ray footprinting mass spectrometry (XFMS) to assess how the solvent accessibility of HCMV Pr changes once it binds to Fab5.

We irradiated our samples with synchrotron X-ray radiation at the Advanced Light Source beamline 3.2.1. which generates hydroxyl radicals *in situ* from the bulk solvent and structure-coordinated water molecules that can covalently label solvent-accessible amino acid side chains. A sample is exposed for varying lengths of time in front of the X-ray beam, which results in a dose range of generated hydroxyl radicals. The extent of oxidative modification is quantified using bottom-up liquid chromatography-tandem mass spectrometry (LC-MS/MS) and the ratio of modified versus unmodified peptide is plotted as a function of exposure time. The result is a dose/response graph for each modified residue detected in the experiment with a hydroxyl reactivity rate constant k_s. By taking the ratio of rate constants at each detected residue between two or more protein states, we can infer structural changes that result in differences in solvent accessibility. This technique is especially useful when paired with cryo-EM because our

atomic models of the Fab5/HCMV Pr complex can be used as the basis to interpret our XFMS results.

In our XFMS data, we see that the Fab5 epitope is protected from solvent exposure upon complex formation, and residues that normally participate in the HCMV Pr dimer interface become solvent-exposed. We also see solvent accessibility changes around the active site when Fab5 binds. The active site-proximal residues captured in our XFMS dataset are not resolved in our cryo-EM structures. By combining our XFMS and cryo-EM datasets, we can gain deeper insights into the dynamics of the HCMV Pr active site in the monomeric state.

<center>**Results**</center>

HCMV Pr Dynamics Revealed by Fab5 Binding

Our XFMS results show that Fab5 binding leads to global HCMV Pr solvent accessibility changes. We detected 20 amino acids that are modified by hydroxyl radicals via LC-MS/MS (**Table 1**). To quantify these changes, we compared the ratio of oxidation rate constants (k_s) for HCMV Pr alone over the Fab5/HCMV Pr complex (**Fig. 2.1a**). One residue in our data set exhibited no change in solvent exposure (ratio equal to one). Many residues were protected from solvent upon Fab5 binding (ratio greater than 1), while some residues became more solvent-exposed (ratio less than one). These residues are evenly dispersed across the HCMV Pr surface (**Fig. 2.1b**).

By mapping XFMS-derived solvent accessibility changes onto both the Fab5/HCMV Pr EM structure and the dimeric HCMV Pr crystal structure (**Fig. 2.2a-2.2b**), we can interpret the effect that Fab5 binding has on HCMV Pr conformation. Residues F123 and Y230 typically participate in the HCMV Pr dimer interface, and Fab5 binding makes them both more solvent exposed. Y230 is not represented in the Fab5/HCMV Pr structure because the interfacial helix α5 is disordered in the complex. Nearby residue Y128 is solvent protected, indicating that there are conformational changes occurring at the dimer interface.

The residues with the greatest degree of protection are in and around the HCMV Pr active site. H157, a member of the catalytic triad, undergoes 2.5-fold solvent protection upon Fab5 binding, and M75, which resides directly behind the active site, is protected 3.38-fold (**Fig. 2.2c**). HCMV Pr residues that are near the Fab5 become

<center>39</center>

solvent protected. P111 directly participates in in the epitope and shows a 2.13-fold decrease in solvent accessibility (**Fig. 2.2d**). W179 makes direct contact with Fab5 in the three classes of the complex that we determined, and it is protected by 2.28-fold. All together, these observations corroborate the allosteric inhibition mechanism of Fab5, and also provide additional information on how the active site is influenced by the HCMV Pr monomer to dimer transition.

M75 and F155 play key roles in HCMV Pr activity

Because residue M75 undergoes the most solvent protection upon Fab5 binding, we hypothesized that its location near the active site undergoes conformational changes between HCMV Pr monomeric and dimeric states. Inspection of several HCMV Pr X-ray crystal structures indicates that F155 is oriented with its sidechain towards M75 and could be a bridge to the active site (**Fig. 2.3a-2.3b**). When HCMV Pr is not bound to substrate, F155 is highly flexible, ranging from 5-11Å away from the M75 sidechain. Overlaying crystal structures of substrate mimetic-bound HCMV Pr reveals that F155 is consistently about 5Å away from M75, which indicates that F155 is sensitive to the active site environment.[32,33] In the ^{1}H-^{13}C HSQC spectrum of unbound HCMV Pr, the peak corresponding to M75 accesses at least four distinct resonance shifts (**Fig. 2.3c**). The observation of multiple peaks indicates that M75 is in several chemical environments, most likely due to different protein conformational states. Mutation of F155 (HCMV F155) causes a shift in M75 and a single HSQC peak, confirming an interaction between the two residues.

We next investigated whether the observed M75 resonances were associated with monomeric or dimeric states of HCMV Pr. Point mutations along the dimer interface

that stabilize either the monomer (HCMV L222D) or the dimer (HCMV S225M) were used to determine ^{1}H-^{13}C chemical shifts of M75 when isolated in each oligomeric state (**Fig. 2.3c**). In the L222D spectrum, M75 shows a major peak that overlaps with peak 3 in the HCMV Pr WT. In the HCMV S225M dimer spectrum, one peak corresponding to M225 partially overlaps with the major peak, which also appears to overlap with resonance 3 in the WT HCMV Pr spectrum. There is also a second resonance that overlaps with resonance 4 in the WT HCMV Pr spectrum, which is not present in the monomer spectrum. We therefore conclude that this peak is specifically associated with the HCMV Pr dimeric state.

While structural evidence shows that M75 and F155 are sensitive to HCMV Pr conformation, we wondered whether they are important for activity as well. By mutating each residue to alanine and performing steady-state kinetics, we show that M75 is important for HCMV Pr activity and F155 is essential (**Fig. 2.3d**). Comparing WT HCMV Pr to HCMV M75A, substrate K_m is not significantly changed (33µM and 44µM, respectively), while both V_{max} and k_{cat} of HCMV M75A (0.004 µM/s, 0.007 s^{-1}) is 4-fold decreased compared to WT HCMV Pr (0.016 µM/s, 0.031 s^{-1}). Calculating k_{cat}/K_m for each protein construct shows a 6-fold decrease in catalytic efficiency between WT HCMV Pr (939 s^{-1}M^{-1}) and HCMV M75A (159 s^{-1}M^{-1}). The HCMV F155A mutant showed no proteolytic activity, so a comparison of kinetic values was not possible in this case.

To determine the effects of mutagenesis on HCMV Pr dimerization, we used SEC to monitor the concentration-dependent monomer/dimer equilibrium as described in chapter 1. WT HCMV Pr elutes as a mixture of monomer and dimer, and increasing protein concentration enhances dimerization (**Fig. 2.3e**). HCMV M75A also elutes as a

mixture of monomer and dimer, but with an increased concentration of monomer. This effect is more pronounced in the case of HCMV F155A, which remains fully monomeric until the highest concentration tested. Based on this, we conclude that both M75 and F155 are important for HCMV Pr dimerization.

Discussion

We performed XFMS concurrently with cryo-EM to investigate the epitope and inhibitory mechanism of Fab5. With cryo-EM, we visualize the epitope in exquisite detail. However, the decreasing resolution further from the Fab5 binding site precluded us from modeling residues of the active site. Led by our XFMS data, we identified a relationship between residues M75, F155, and HCMV Pr activity. Sequence alignment of all HHV Prs shows that F155 is fully conserved across the HHV Pr family (**Fig. 2.4a**). While M75 is not conserved, residues at this location contain bulky hydrophobic sidechains. Inspection of the crystal structures of Kaposi's Sarcoma-associated herpesvirus (KSHV), Epstein-Barr virus (EBV), Herpes Simplex Virus type 2 (HSV-2) and Varicella-zoster virus (VZV) proteases indicates structural conservation of sidechain interactions at this location (**Fig. 2.4b**). This conservation suggests that M75 and F155 play similar roles in homologs to mediate dimerization and activity.

These XFMS data alone did not allow us to confidently determine the Fab5 epitope. However, since these experiments were performed, upgrades in the beamline 3.2.1 and 3.2.2 endstations, along with more sophisticated LC-MS/MS data processing strategies, led to numerous successful antibody epitope mapping endeavors using XFMS.[27,34] Furthermore, combining XFMS with cryo-EM is proving to be a powerful way

to study protein dynamics because XFMS can report on structural features that are too

flexible for structure determination.[35]
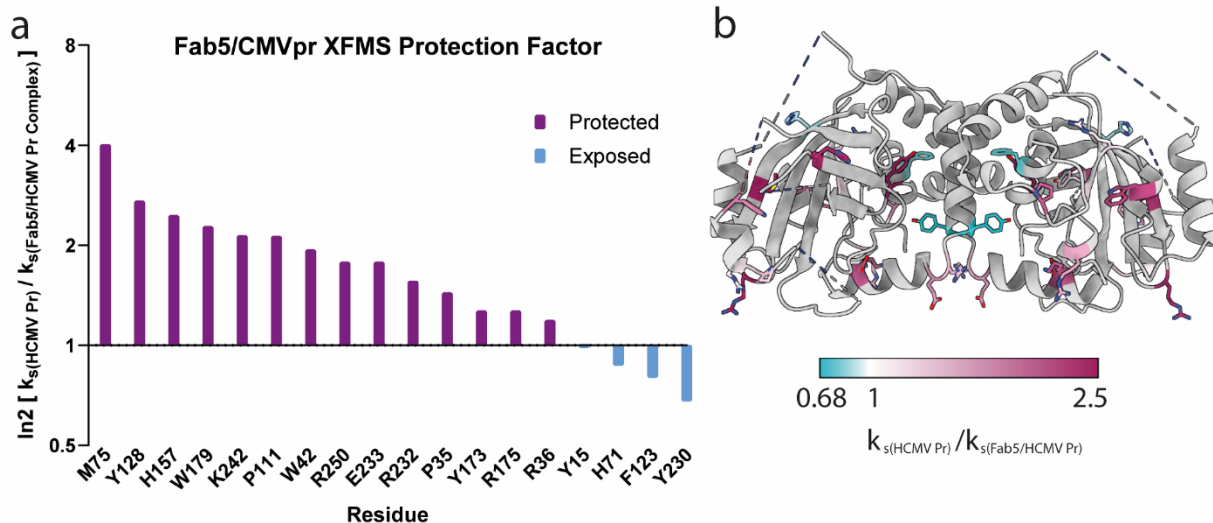
Figure 2.1: XFMS results mapped onto HCMV Pr crystal structure. a) HCMV Pr residue-specific changes in solvent accessibility upon Fab5/HCMV Pr complex formation. The height of each column corresponds to the ratio of hydroxyl radical reactivity rate of HCMV Pr alone over the rate of that of the Fab5/HCMV Pr complex. Residues with values above 1 are protected from solvent, and residues with values below 1 are more solvent-exposed. b) XFMS data mapped onto HCMV Pr crystal structure (PDB:1CMV). Scale bar is the same for all structures shown in chapter 2.
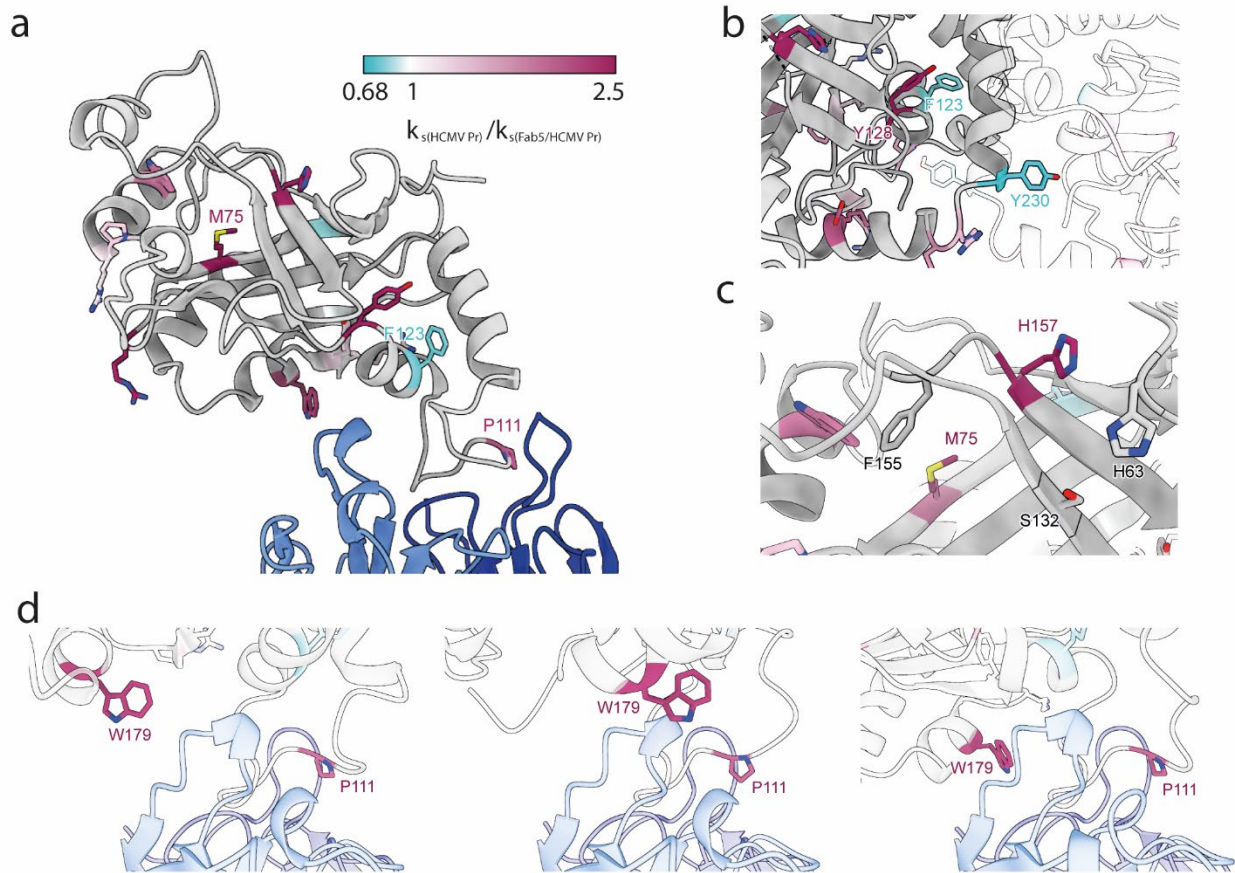
Figure 2.2: XFMS mapped onto Fab5/HCMV Pr complex. a) Oxidation rate changes between HCMV Pr and Fab5/HCMV Pr complex mapped onto corresponding residues on the Fab5/HCMV Pr cryo-EM model from Class One. b) XFMS data mapped onto an HCMV Pr dimeric crystal structure with the dimer interface highlighted. One monomer is translucent. c) XFMS data mapped onto the HCMV Pr active site area. d) a view of the Fab5/HCMV Pr interface with residues P111 and W179 highlighted.
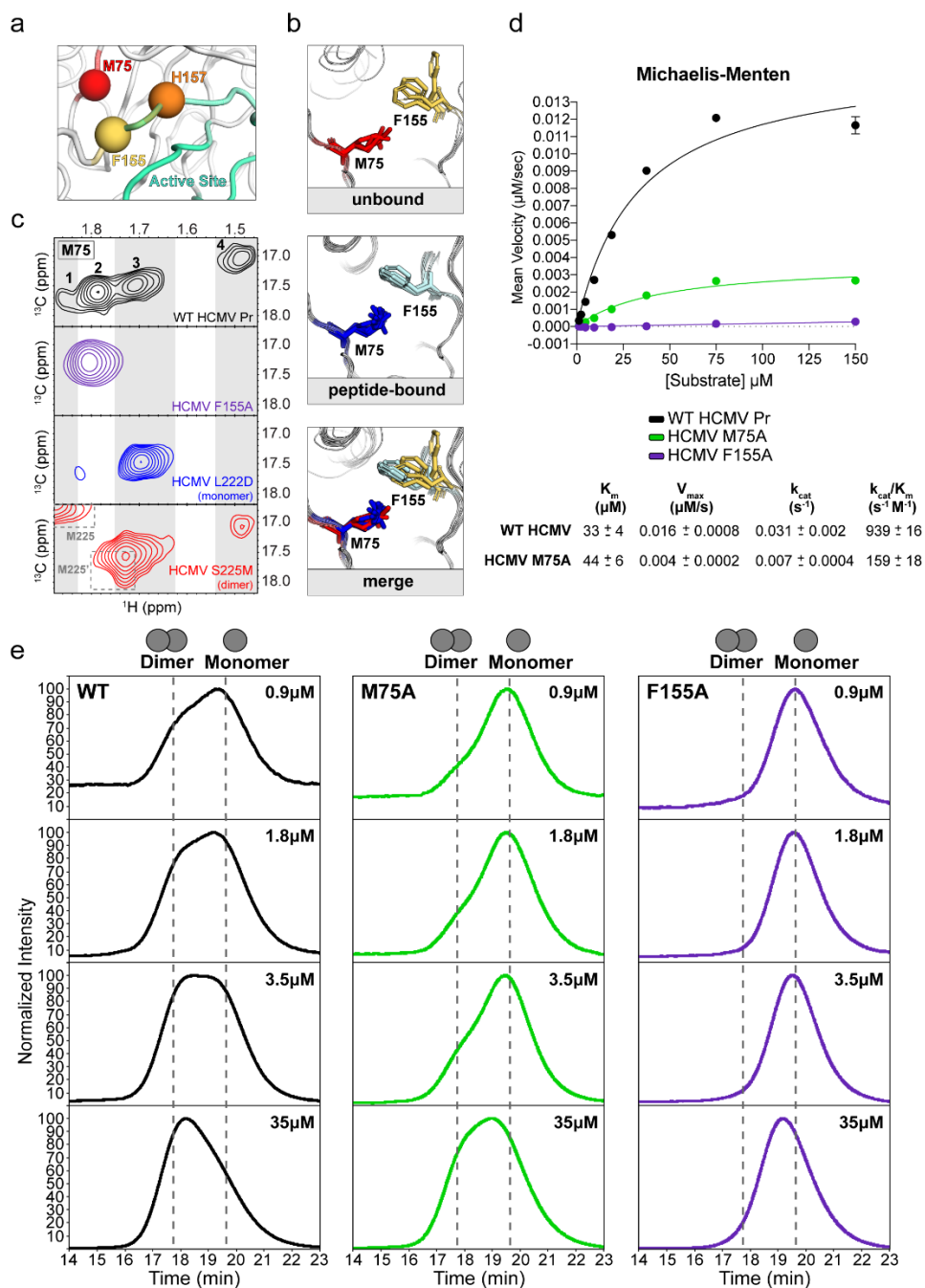
Figure 2.3: M75 and F155 are important for activity and dimerization. a) M75 (red) is located behind F155 (yellow), which is nearby the catalytic residue H157 (orange) and the active site (greencyan). b) Top: Overlays of every chain in the asymmetric unit of several apo HCMV Pr crystal structures (PDBs: 1CMV, 1LAY, 1WPO). F155 was not resolved in some of the inspected chains, and is not depicted in those cases. Middle: Overlays of every chain in the asymmetric unit of several substrate-mimetic bound HCMV Pr crystal structures (PDBs: 1NJT, 1NKK, 1NKM, 1NJU, 2WPO). Bottom: All overlays are merged. c) The 1H-13C resonances associated with M75 are shown for WT HCMV Pr (black), HCMV F155A (purple), HCMV L222D (blue) and HCMV S225M (red). d) The catalytic efficiency of WT HCMV Pr (black), HCMV M75A (green) and HCMV F155A (purple) was determined. (figure caption continued on next page)

(figure caption continued from the previous page) Data are depicted in triplicate from (continued from previous page) technical replicates as the mean ± standard deviation. e) SEC was used to monitor the monomer/dimer equilibrium over a concentration range of WT HCMV Pr (black) HCMV M75A (green) and HCMV F155A (purple). The monomer/dimer peaks are labeled for reference.

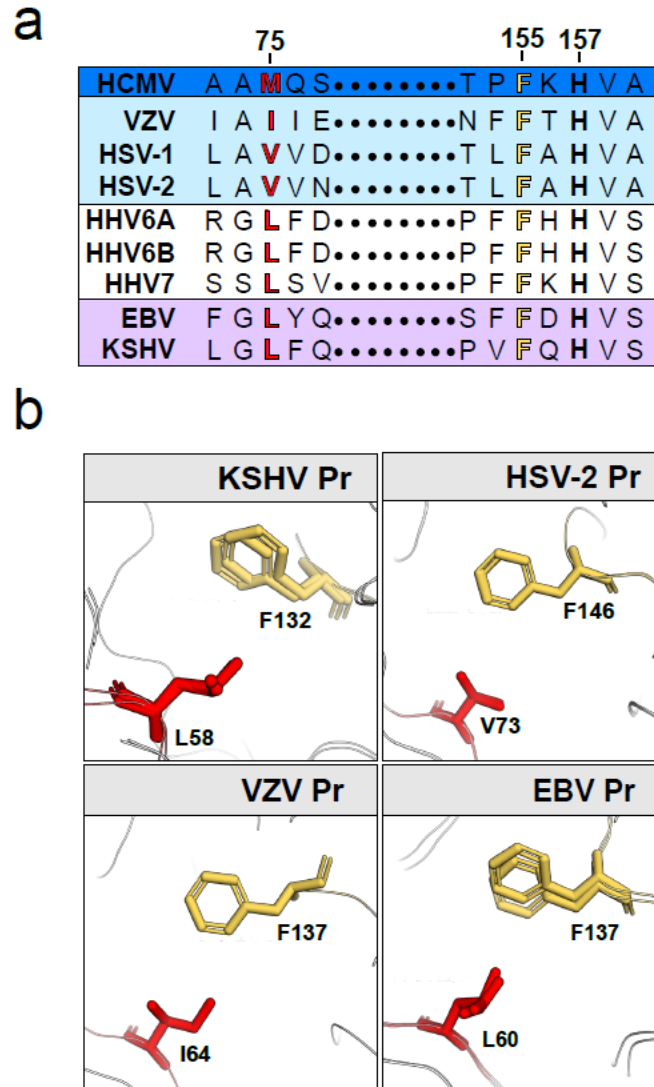

Figure 2.4: M75 and F155 conservation. a) A sequence alignment for all HHV Prs is shown. M75 (red) is type-conserved as a bulky hydrophobic residue, and F155 (yellow) is absolutely conserved. b) We overlaid the chains in X-ray crystal structures for KSHV, HSV-2, VZV and EBV Prs (PDBs 1FL1, 1AT3, 1VZV, 1O6E). Residues corresponding to M75 are red, residues corresponding to F155 are yellow.

Tables

Table 2.1: List of peptides used in XFMS analysis. Oxidized residues in the XFMS dataset are listed with accompanying peptide. The oxidation rate k_s for unbound HCMV Pr (knative) and the Fab5/HCV Pr complex (kcomplex) are given, as well as the ratio (knavtive/kcomplex).

Residue	Peptide	knative	kcomplex	knative/ kcomplex
Y15	DEQQSQAVAPVYVGGFLAR	1.05	1.06	0.99
P35	DEAELLLPR	1.30	0.90	1.44
R36	DEAELLLPR	1.51	1.27	1.19
W42	DVVEHWLHAQGQGQPSL SVALPLNINH	4.03	2.08	1.94
H71	DTAVVGHVAAMQSVR	8.37	9.62	0.87
M75	DDTAVVGHVAAMQSVR	10.83	3.65	2.97
M75*	DDTAVVGHVAAMQSVR	4.66	2.31	2.02
H71 + M75*	DDTAVVGHVAAMQSVR	4.43	0.28	15.82
R79	TAVVGHVAAMQSVR	4.39	1.30	3.38
M75 + R79*	DDTAVVGHVAAMQSVR	1.86	0.21	8.86
P111	LVSRGPVSPLQP	1.92	0.90	2.13
F123	VVEFLSGSYAGLSLSSR	0.32	0.40	0.80
Y128	VVEFLSGSYAGLSLSSR	0.49	0.18	2.72
H157	HVALCSVGR	0.32	0.13	2.46
Y173	GTLAVYGR	0.14	0.11	1.27
R175	GTLAVYGR	0.14	0.11	1.27
P177 + W179*	DPEWVTQR	0.96	0.55	1.75
W179	DPEWVTQR	3.69	1.62	2.28
Y230	DALYIR	0.97	1.43	0.68
R232	DALYIRE	0.39	0.25	1.56
E233	DALYIRE	0.91	0.51	1.78
D241	DKQLVGVTE	1.50	0.70	2.14
K242	DKQLVGVTE	1.50	0.70	2.14
R250	QLVGVTER	1.23	0.69	1.78
	*Not included in final analysis			

Materials and Methods

Protein Purification and Steady-State Kinetics were performed as described in Chapter 1.

HSQC NMR: Selective 13C-ILVM labeled HCMV Pr, HCMV L222D, HCMV S225M or HCMV F155A was diluted to ~80-100 μM in a buffer containing 25 mM potassium phosphate pH 7.0, 150 mM KCl, 0.1 mM EDTA, 5 mM dithiothreitol and 10% deuterium oxide. All NMR spectra were acquired at 300 K on either a Bruker Avance DRX 500 MHz spectrometer equipped with a QCI CryoProbe and a 60-slot B-ACS sample changer or a Bruker Avance AV 800 MHz spectrometer equipped with a TXI CryoProbe and a 16-slot SE Lite sample changer. Spectral processing analysis was performed with NMRpipe and NMRFAM-Sparky.35 Peak assignments were previously determined

Size-exclusion chromatography: WT HCMV Pr, HCMV M75A or HCMV F155A were diluted (0.9 μM, 1.8 μM, 3.5 μM or 35 μM final concentration) into buffer containing 25 mM potassium phosphate pH 8.0, 150 mM KCl, 0.1 mM EDTA, 10% glycerol and 1 mM β-mercaptoethanol then incubated at room temperature for 1-7 h. Data were acquired and analyzed as previously described

XFMS: HCMV Pr samples with or without Fab **5** were prepared at 2 micromolar. Protein concentrations and beam parameters were optimized using an Alexa-488 fluorophore assay. Samples were exposed for between 0–150 ms to a focused synchrotron X-ray white beam at beamline 3.2.1 at the Advanced Light Source in Berkeley, CA. Samples were immediately quenched post exposure and overnight digestion with trypsin or glu-c was initiated on the same day. Oxidation sites were detected by liquid chromatography-tandem mass spectrometry (LC-MS/MS) carried out at Joint BioEnergy Institute,

Berkeley, CA and analyzed as previously described.[27] The amount of unmodified peptide is calculated by dividing the unmodified peak area by the sum of unmodified and modified peak areas. As the dose of X-ray radiation is increased, the fraction of unmodified peptide decreases, and fitting this dose-response relationship to single exponential decay reveals the rate of footprinting (k_s). This rate is dependent on both the intrinsic reactivity of the specific side chain and its accessibility to solvent. The ratio R of the rate constants at specific amino acid sites between samples reveals changes in relative solvent accessibility. The R values determined in this study were mapped onto the presented structures for comparative structural analysis.

References

(1) Gable, J. E.; Acker, T. M.; Craik, C. S. Current and Potential Treatments for Ubiquitous but Neglected Herpesvirus Infections. *Chem. Rev.* **2014**, *114* (22), 11382–11412. https://doi.org/10.1021/cr500255e.

(2) Francis, S. S.; Wallace, A. D.; Wendt, G. A.; Li, L.; Liu, F.; Riley, L. W.; Kogan, S.; Walsh, K. M.; de Smith, A. J.; Dahl, G. V.; Ma, X.; Delwart, E.; Metayer, C.; Wiemels, J. L. In Utero Cytomegalovirus Infection and Development of Childhood Acute Lymphoblastic Leukemia. *Blood* **2017**, *129* (12), 1680–1684. https://doi.org/10.1182/blood-2016-07-723148.

(3) Rawlinson, W. D.; Boppana, S. B.; Fowler, K. B.; Kimberlin, D. W.; Lazzarotto, T.; Alain, S.; Daly, K.; Doutré, S.; Gibson, L.; Giles, M. L.; Greenlee, J.; Hamilton, S. T.; Harrison, G. J.; Hui, L.; Jones, C. A.; Palasanthiran, P.; Schleiss, M. R.; Shand, A. W.; van Zuylen, W. J. Congenital Cytomegalovirus Infection in Pregnancy and the Neonate: Consensus Recommendations for Prevention, Diagnosis, and Therapy. *Lancet Infect. Dis.* **2017**, *17* (6), e177–e188. https://doi.org/10.1016/S1473-3099(17)30143-3.

(4) McIntosh, M.; Hauschild, B.; Miller, V. Human Cytomegalovirus and Transplantation: Drug Development and Regulatory Issues. *J. Virus Erad.* **2016**, *2* (3), 143.

(5) El Helou, G.; Razonable, R. R. Letermovir for the Prevention of Cytomegalovirus Infection and Disease in Transplant Recipients: An Evidence-Based Review. *Infect. Drug Resist.* **2019**, *12*, 1481–1491. https://doi.org/10.2147/IDR.S180908.

(6) Lischka, P.; Michel, D.; Zimmermann, H. Characterization of Cytomegalovirus Breakthrough Events in a Phase 2 Prophylaxis Trial of Letermovir (AIC246, MK 8228). *J. Infect. Dis.* **2016**, *213* (1), 23–30. https://doi.org/10.1093/infdis/jiv352.

(7) Gao, M.; Matusick-Kumar, L.; Hurlburt, W.; DiTusa, S. F.; Newcomb, W. W.; Brown, J. C.; P J McCann, 3rd; Deckman, I.; Colonno, R. J. The Protease of Herpes Simplex Virus Type 1 Is Essential for Functional Capsid Formation and Viral Growth. *J. Virol.* **1994**, *68* (6), 3702. https://doi.org/10.1128/jvi.68.6.3702-3712.1994.

(8) Dunn, W.; Trang, P.; Khan, U.; Zhu, J.; Liu, F. RNase P-Mediated Inhibition of Cytomegalovirus Protease Expression and Viral DNA Encapsidation by Oligonucleotide External Guide Sequences. *Proc. Natl. Acad. Sci. U. S. A.* **2001**, *98* (26), 14831–14836. https://doi.org/10.1073/pnas.261560598.

(9) Batra, R.; Khayat, R.; Tong, L. Molecular Mechanism for Dimerization to Regulate the Catalytic Activity of Human Cytomegalovirus Protease. *Nat. Struct. Biol.* **2001**, *8* (9), 810–817. https://doi.org/10.1038/nsb0901-810.

(10) Waxman, L.; Darke, P. L. The Herpesvirus Proteases as Targets for Antiviral Chemotherapy. *Antivir. Chem. Chemother.* **2000**, *11* (1), 1–22. https://doi.org/10.1177/095632020001100101.

(11) Darke, P. L.; Cole, J. L.; Waxman, L.; Hall, D. L.; Sardana, M. K.; Kuo, L. C. Active Human Cytomegalovirus Protease Is a Dimer. *J. Biol. Chem.* **1996**, *271* (13), 7445–7449. https://doi.org/10.1074/jbc.271.13.7445.

(12) Nomura, A. M.; Marnett, A. B.; Shimba, N.; Dötsch, V.; Craik, C. S. Induced Structure of a Helical Switch as a Mechanism to Regulate Enzymatic Activity. *Nat. Struct. Mol. Biol.* **2005**, *12* (11), 1019–1020. https://doi.org/10.1038/nsmb1006.

(13)   Zühlsdorf, M.; Werten, S.; Klupp, B. G.; Palm, G. J.; Mettenleiter, T. C.; Hinrichs, W. Dimerization-Induced Allosteric Changes of the Oxyanion-Hole Loop Activate the Pseudorabies Virus Assemblin pUL26N, a Herpesvirus Serine Protease. *PLoS Pathog.* **2015**, *11* (7), e1005045. https://doi.org/10.1371/journal.ppat.1005045.

(14)   Shahian, T.; Lee, G. M.; Lazic, A.; Arnold, L. A.; Velusamy, P.; Roels, C. M.; Guy, R. K.; Craik, C. S. Inhibition of a Viral Enzyme by a Small-Molecule Dimer Disruptor. *Nat. Chem. Biol.* **2009**, *5* (9), 640–646. https://doi.org/10.1038/nchembio.192.

(15)   Lee, G. M.; Shahian, T.; Baharuddin, A.; Gable, J. E.; Craik, C. S. Enzyme Inhibition by Allosteric Capture of an Inactive Conformation. *J. Mol. Biol.* **2011**, *411* (5), 999–1016. https://doi.org/10.1016/j.jmb.2011.06.032.

(16)   Gable, J. E.; Lee, G. M.; Jaishankar, P.; Hearn, B. R.; Waddling, C. A.; Renslo, A. R.; Craik, C. S. Broad-Spectrum Allosteric Inhibition of Herpesvirus Proteases. *Biochemistry* **2014**, *53* (28), 4648. https://doi.org/10.1021/bi5003234.

(17)   Acker, T. M.; Gable, J. E.; Bohn, M.-F.; Jaishankar, P.; Thompson, M. C.; Fraser, J. S.; Renslo, A. R.; Craik, C. S. Allosteric Inhibitors, Crystallography, and Comparative Analysis Reveal Network of Coordinated Movement across Human Herpesvirus Proteases. *J. Am. Chem. Soc.* **2017**, *139* (34), 11650–11653. https://doi.org/10.1021/jacs.7b04030.

(18)   Hulce, K. R.; Jaishankar, P.; Lee, G. M.; Bohn, M.-F.; Connelly, E. J.; Wucherer, K.; Ongpipattanakul, C.; Volk, R. F.; Chuo, S.-W.; Arkin, M. R.; Renslo, A. R.; Craik, C. S. Inhibiting a Dynamic Viral Protease by Targeting a Non-Catalytic Cysteine. *Cell Chem. Biol.* **2022**, *29* (5), 785-798.e19. https://doi.org/10.1016/j.chembiol.2022.03.007.

(19)   Basu, K.; Green, E. M.; Cheng, Y.; Craik, C. S. Why Recombinant Antibodies —

Benefits and Applications. *Curr. Opin. Biotechnol.* **2019**, *60*, 153–158.

https://doi.org/10.1016/j.copbio.2019.01.012.

(20)   Farady, C. J.; Egea, P. F.; Schneider, E. L.; Darragh, M. R.; Craik, C. S. Structure

of an Fab-Protease Complex Reveals a Highly Specific Non-Canonical Mechanism

of Inhibition. *J. Mol. Biol.* **2008**, *380* (2), 351–360.

https://doi.org/10.1016/j.jmb.2008.05.009.

(21)   Lescar, J.; Brynda, J.; Rezacova, P.; Stouracova, R.; Riottot, M. M.; Chitarra, V.;

Fabry, M.; Horejsi, M.; Sedlacek, J.; Bentley, G. A. Inhibition of the HIV-1 and HIV-2

Proteases by a Monoclonal Antibody. *Protein Sci. Publ. Protein Soc.* **1999**, *8* (12),

2686. https://doi.org/10.1110/ps.8.12.2686.

(22)   Fukuoka, Y.; Schwartz, L. B. The B12 Anti-Tryptase Monoclonal Antibody

Disrupts the Tetrameric Structure of Heparin-Stabilized β-Tryptase to Form

Monomers That Are Inactive at Neutral pH and Active at Acidic pH. *J. Immunol.*

Baltim. Md 1950 **2006**, *176* (5), 3165. https://doi.org/10.4049/jimmunol.176.5.3165.

(23)   Schaefer, M.; Buchmueller, A.; Dittmer, F.; Straßburger, J.; Wilmen, A. Allosteric

Inhibition as a New Mode of Action for BAY 1213790, a Neutralizing Antibody

Targeting the Activated Form of Coagulation Factor XI. *J. Mol. Biol.* **2019**, *431* (24),

4817–4833. https://doi.org/10.1016/j.jmb.2019.09.008.

(24)   Sudol, K. L.; Mastrangelo, M. A.; Narrow, W. C.; Frazer, M. E.; Levites, Y. R.;

Golde, T. E.; Federoff, H. J.; Bowers, W. J. Generating Differentially Targeted

Amyloid-Beta Specific Intrabodies as a Passive Vaccination Strategy for Alzheimer's

Disease. *Mol. Ther. J. Am. Soc. Gene Ther.* **2009**, *17* (12), 2031–2040.
https://doi.org/10.1038/mt.2009.174.

(25)   Rodrigues, G. A.; Shalaev, E.; Karami, T. K.; Cunningham, J.; Slater, N. K. H.;
Rivers, H. M. Pharmaceutical Development of AAV-Based Gene Therapy Products
for the Eye. *Pharm. Res.* **2018**, *36* (2), 29. https://doi.org/10.1007/s11095-018-2554-
7.

(26)   Kim, J.; Stroud, R. M.; Craik, C. S. Rapid Identification of Recombinant Fabs That
Bind to Membrane Proteins. *Methods* **2011**, *55* (4), 303–309.
https://doi.org/10.1016/j.ymeth.2011.09.012.

(27)   Sevillano, N.; Bohn, M. F.; Zimanyi, M.; Chen, Y.; Petzold, C.; Gupta, S.; Ralston,
C. Y.; Craik, C. S. Structure of an Affinity-Matured Inhibitory Recombinant Fab
against Urokinase Plasminogen Activator Reveals Basis of Potency and Specificity.
Biochim. Biophys. Acta Proteins Proteomics **2021**, *1869* (2), 140562.
https://doi.org/10.1016/j.bbapap.2020.140562.

(28)   Jin, M.; Seed, R. I.; Cai, G.; Shing, T.; Wang, L.; Ito, S.; Cormier, A.; Wankowicz,
S. A.; Jespersen, J. M.; Baron, J. L.; Carey, N. D.; Campbell, M. G.; Yu, Z.; Tang, P.
K.; Cossio, P.; Wen, W.; Lou, J.; Marks, J.; Nishimura, S. L.; Cheng, Y. Dynamic
Allostery Drives Autocrine and Paracrine TGF-β Signaling. *Cell* **2024**, *187* (22),
6200-6219.e23. https://doi.org/10.1016/j.cell.2024.08.036.

(29)   Bern, D.; Tobi, D. The Effect of Dimerization and Ligand Binding on the Dynamics
of Kaposi's Sarcoma-associated Herpesvirus Protease. *Proteins* **2022**, *90* (6), 1267.
https://doi.org/10.1002/prot.26307.

(30)   Wu, M.; Lander, G. C. How Low Can We Go? Structure Determination of Small Biological Complexes Using Single-Particle Cryo-EM. *Curr. Opin. Struct. Biol.* **2020**, *64*, 9–16. https://doi.org/10.1016/j.sbi.2020.05.007.

(31)   Kung, J. E.; Johnson, M. C.; Jao, C. C.; Arthur, C. P.; Tegunov, D.; Rohou, A.; Sudhamsu, J. Disulfi de Constrained Fabs Overcome Target Size Limitation for High-Resolution Single-Particle Cryo-EM. *bioRxiv* **2024**, 2024.05.10.593593. https://doi.org/10.1101/2024.05.10.593593.

(32)   Tong, L.; Qian, C.; Massariol, M. J.; Déziel, R.; Yoakim, C.; Lagacé, L. Conserved Mode of Peptidomimetic Inhibition and Substrate Recognition of Human Cytomegalovirus Protease. *Nat. Struct. Biol.* **1998**, *5* (9), 819–826. https://doi.org/10.1038/1860.

(33)   Khayat, R.; Batra, R.; Qian, C.; Halmos, T.; Bailey, M.; Tong, L. Structural and Biochemical Studies of Inhibitor Binding to Human Cytomegalovirus Protease. *Biochemistry* **2003**, *42* (4), 885–891. https://doi.org/10.1021/bi027045s.

(34)   Kristensen, L. G.; Gupta, S.; Chen, Y.; Petzold, C. J.; Ralston, C. Y. Residue-Specific Epitope Mapping of the PD-1/Nivolumab Interaction Using X-Ray Footprinting Mass Spectrometry. *Antibodies* **2024**, *13* (3), 77. https://doi.org/10.3390/antib13030077.

(35)   Schoof, M.; Faust, B.; Saunders, R. A.; Sangwan, S.; Rezelj, V.; Hoppe, N.; Boone, M.; Billesbølle, C. B.; Puchades, C.; Azumaya, C. M.; Kratochvil, H. T.; Zimanyi, M.; Deshpande, I.; Liang, J.; Dickinson, S.; Nguyen, H. C.; Chio, C. M.; Merz, G. E.; Thompson, M. C.; Diwanji, D.; Schaefer, K.; Anand, A. A.; Dobzinski, N.; Zha, B. S.; Simoneau, C. R.; Leon, K.; White, K. M.; Chio, U. S.; Gupta, M.; Jin, M.;

Li, F.; Liu, Y.; Zhang, K.; Bulkley, D.; Sun, M.; Smith, A. M.; Rizo, A. N.; Moss, F.; Brilot, A. F.; Pourmal, S.; Trenker, R.; Pospiech, T.; Gupta, S.; Barsi-Rhyne, B.; Belyy, V.; Barile-Hill, A. W.; Nock, S.; Liu, Y.; Krogan, N. J.; Ralston, C. Y.; Swaney, D. L.; García-Sastre, A.; Ott, M.; Vignuzzi, M.; QCRG Structural Biology Consortium; Walter, P.; Manglik, A. An Ultrapotent Synthetic Nanobody Neutralizes SARS-CoV-2 by Stabilizing Inactive Spike. *Science* **2020**, *370* (6523), 1473–1479. https://doi.org/10.1126/science.abe3255.

Publishing Agreement

It is the policy of the University to encourage open access and broad distribution of all theses, dissertations, and manuscripts. The Graduate Division will facilitate the distribution of UCSF theses, dissertations, and manuscripts to the UCSF Library for open access and distribution. UCSF will make such theses, dissertations, and manuscripts accessible to the public and will take reasonable steps to preserve these works in perpetuity.

I hereby grant the non-exclusive, perpetual right to The Regents of the University of California to reproduce, publicly display, distribute, preserve, and publish copies of my thesis, dissertation, or manuscript in any form or media, now existing or later derived, including access online for teaching, research, and public service purposes.

DocuSigned by:

Marcell Zimanyi

F003400F7F6A4AC...

Author Signature

12/8/2024

Date